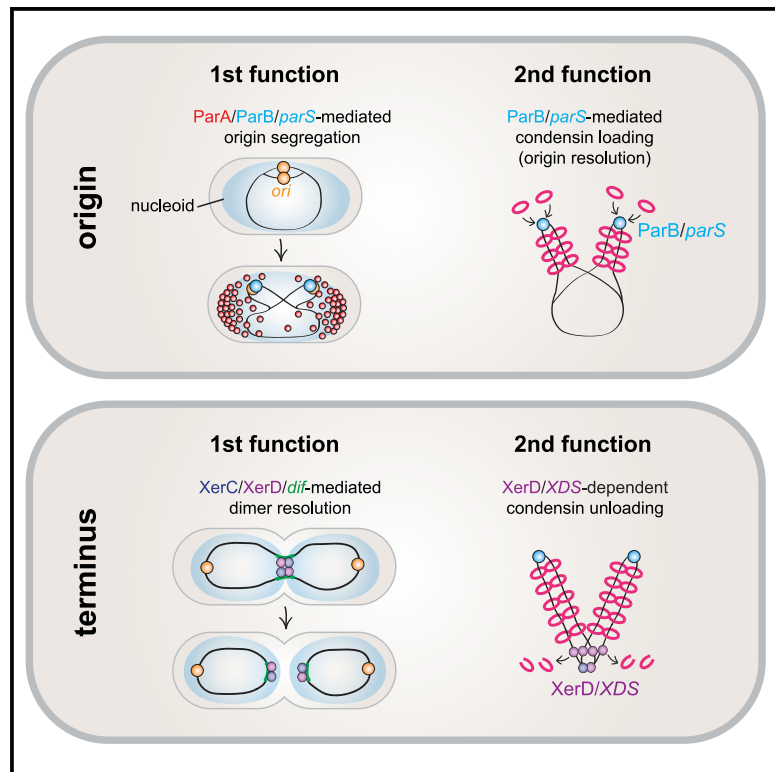


XerD unloads bacterial SMC complexes at the replication terminus

Graphical Abstract



Authors

Xheni Karaboja, Zhongqing Ren,
Hugo B. Brandão, Payel Paul,
David Z. Rudner, Xindan Wang

Correspondence

rudner@hms.harvard.edu (D.Z.R.),
xindan@indiana.edu (X.W.)

In Brief

SMC condensin complexes are loaded at replication origins by the partitioning protein ParB. Karaboja et al. show that condensins are unloaded when they reach the terminus by the recombinase XerD. Thus, broadly conserved factors that act at the origin and terminus load and unload SMC complexes that travel between them.

Highlights

- *Bacillus subtilis* XerD binds novel sites in the replication terminus region
- SMC complexes loaded at the origin are unloaded by XerD at the terminus
- XerD functions as a site-specific unloader of translocating SMC complexes
- ParB-mediated condensin loading and XerD-mediated condensin unloading are conserved

Article

XerD unloads bacterial SMC complexes at the replication terminus

Xheni Karaboja,¹ Zhongqing Ren,¹ Hugo B. Brandão,² Payel Paul,¹ David Z. Rudner,^{3,*} and Xindan Wang^{1,4,*}

¹Department of Biology, Indiana University, Bloomington, IN 47405, USA

²Graduate Program in Biophysics, Harvard University, Cambridge, MA 02138, USA

³Department of Microbiology, Harvard Medical School, Boston, MA 02115, USA

⁴Lead contact

*Correspondence: rudner@hms.harvard.edu (D.Z.R.), xindan@indiana.edu (X.W.)

<https://doi.org/10.1016/j.molcel.2020.12.027>

SUMMARY

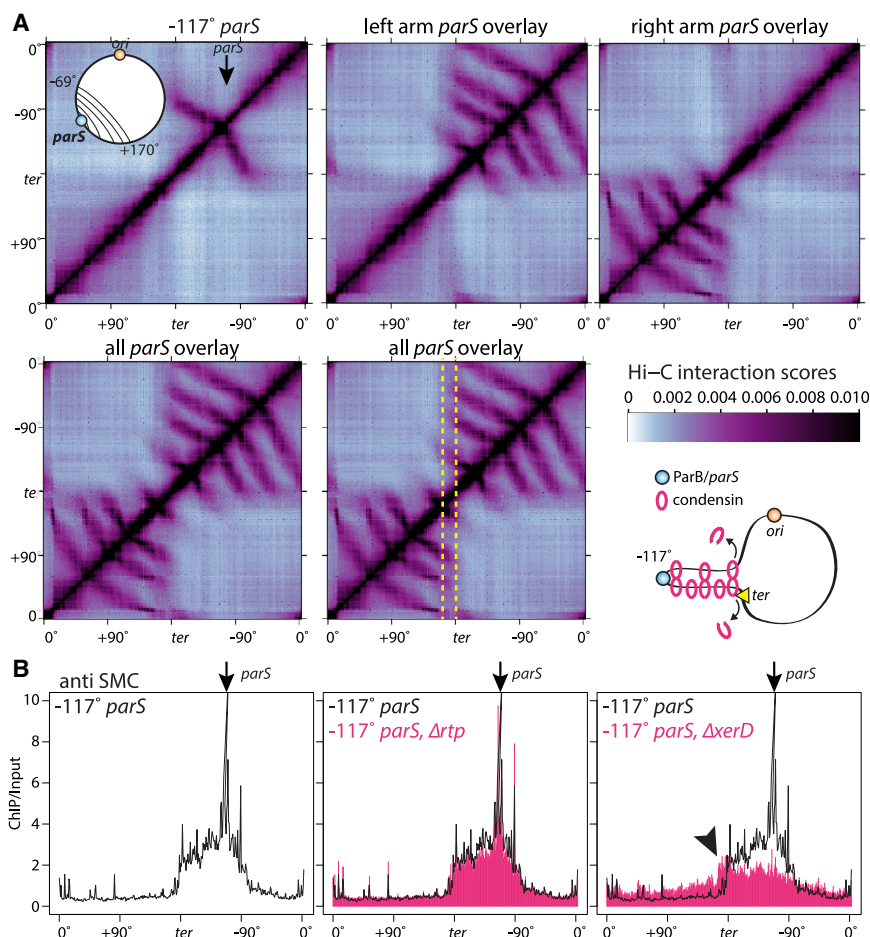
Bacillus subtilis structural maintenance of chromosomes (SMC) complexes are topologically loaded at centromeric sites adjacent to the replication origin by the partitioning protein ParB. These ring-shaped ATPases then translocate down the left and right chromosome arms while tethering them together. Here, we show that the site-specific recombinase XerD, which resolves chromosome dimers, is required to unload SMC tethers when they reach the terminus. We identify XerD-specific binding sites in the terminus region and show that they dictate the site of unloading in a manner that depends on XerD but not its catalytic residue, its partner protein XerC, or the recombination site *dif*. Finally, we provide evidence that ParB and XerD homologs perform similar functions in *Staphylococcus aureus*. Thus, two broadly conserved factors that act at the origin and terminus have second functions in loading and unloading SMC complexes that travel between them.

INTRODUCTION

Structural maintenance of chromosomes (SMC) complexes play central roles in organizing genomes in all domains of life (Hirano, 2016; Uhlmann, 2016; Yatskevich et al., 2019). Recent studies in bacteria and eukaryotes have provided evidence for a model in which these ring-shaped ATPases structure chromosomes by extruding DNA loops (Hassler et al., 2018; Marko et al., 2019; Yatskevich et al., 2019). In this model, SMC complexes are topologically loaded onto DNA and then translocate away from their loading site, processively enlarging a chromosome loop. Loop extrusion provides an explanation of how these complexes resolve newly replicated origins in bacteria, linearly compact and resolve sister chromatids in eukaryotic prophase, and generate topological associating domains (TADs) during interphase. Although factors that load SMC complexes onto DNA at specific sites along the chromosome have been well characterized (Yatskevich et al., 2019), site-specific unloaders that could specify domain boundaries have only been recently hinted at (Lioy et al., 2018; Mäkelä and Sherratt, 2020; Nolivos et al., 2016). Here, we report that the XerD recombinase is required for site-specific unloading of bacterial SMC complexes at the replication terminus.

In most bacteria, a small set of broadly conserved factors act at the origin and terminus to promote the resolution and segregation of replicated chromosomes (Badrinarayanan et al., 2015; Reyes-Lamothe et al., 2012). The ParAB/parS system plays a

central role in segregating newly replicated origins. ParB binds site-specifically to centromeric sequences called *parS* adjacent to the replication origin, and ParA ATPases act on these complexes, promoting their directed movement toward opposite cell poles. The XerCD/dif system functions at the terminus to resolve fully replicated chromosomes (Lesterlin et al., 2004; Midonet and Barre, 2014). XerC and XerD have been extensively studied in *E. coli*, although some of the findings have been reproduced in *B. subtilis* and other organisms (Blakely et al., 1993; Cornet et al., 1997; Jensen, 2006; Sciochetti et al., 1999, 2001; Val et al., 2008). XerC and XerD are site-specific recombinases that bind a recombination site called *dif* and catalyze the resolution of chromosome dimers that arise as a result of homologous recombination during replication (Blakely et al., 1993; Cornet et al., 1997; Sciochetti et al., 1999, 2001). The *dif* site is located in the replication terminus region, as defined by the sites bound by the replication termination protein RTP (Duggin et al., 2008), which is segregated by the SpoIIIE/FtsK family of proteins at the time of cell division (Crozat et al., 2014; Sherratt et al., 2010). Repeated rounds of XerCD-mediated recombination at *dif* have also been shown to remove interlinks (known as catenanes) between sister chromosomes (Grainge et al., 2007; Ip et al., 2003; Shimokawa et al., 2013). Studies in a growing number of bacteria have revealed that the ParB/parS nucleoprotein complex performs a second function: the recruitment and loading of the bacterial SMC complex (Böhml et al., 2020; Gruber and Errington, 2009; Minnen et al., 2011; Sullivan et al., 2009;



Tran et al., 2017). Once loaded, SMC complexes travel from origin-proximal *parS* sites to the terminus while tethering the left and right chromosome arms together (Wang et al., 2015, 2017). Thus, these complexes generate a single chromosome loop that draws sister chromosomes in on themselves and away from each other and likely facilitate the removal of pre-catenanes by Topoisomerase IV (Bürmann and Gruber, 2015; Marko, 2009). The fate of SMC complexes upon arrival at the terminus has been unclear.

Chromatin immunoprecipitation sequencing (ChIP-seq) and Hi-C studies in *B. subtilis* suggest that loop extrusion by SMC complexes is mediated by two “handcuffed” rings (Brandão et al., 2019; Wang et al., 2015). Biochemical studies indicate that the *E. coli* MukBEF complex, an analog of SMC complexes, indeed forms dimers (Badrinarayanan et al., 2012; Rajasekar et al., 2019). In this model, separate SMC complexes encircle the DNA on either side of *parS* and translocate away from the loading site as a dimer. If correct, the tethered rings would remain topologically associated with the DNA when they reach the terminus and might require an active mechanism to unload them. Here, we show that the XerD recombinase has a heretofore unrecognized second function in unloading bacterial SMC complexes at the terminus. We identify XerD-specific binding sites in the terminus region and show that these binding sites

and XerD but not XerC or *dif* are required for site-specific unloading of SMC complexes. We identify similar binding sites in *S. aureus* and provide evidence that ParB and XerD have similar loading and unloading functions in this bacterium. Thus, the loading and unloading of SMC complexes are mediated by two broadly conserved factors: one involved in origin segregation, the other in terminus resolution. Similar site-specific unloading activities could modulate eukaryotic SMC complexes during interphase and mitosis.

RESULTS

B. subtilis cells lacking their endogenous *parS* sites and harboring a single ectopic *parS* site juxtapose large tracks of DNA flanking the ectopic site in a ParB- and SMC-dependent manner (Wang et al., 2015, 2017) (Figures 1A and S1A). Intriguingly, the DNA juxtaposition never extends beyond a ~300 kb region surrounding the replication terminus, regardless of where *parS* is inserted (Figure 1A). Similarly, SMC complexes are specifically enriched along the juxtaposed DNA and enrichment does not extend beyond the terminus region (Wang et al., 2017) (Figures 1B and S1B).

To investigate whether any of the factors that act in the terminus region also function to prevent SMC from translocating

Molecular Cell

Article



beyond it, we analyzed SMC enrichment in a set of mutants harboring a single *parS* site at -117° . We performed ChIP-seq on cells lacking the replication termination protein RTP, which binds Ter sites and ensures replication terminates within a defined region (Duggin et al., 2008); the two DNA translocases (SpollIE and SftA) (Kaimer et al., 2011) that act at the division septum to segregate terminus-proximal DNA into the appropriate daughter cell; and the site-specific recombinases XerC (CodV) and XerD (RipX) and the recombination site *dif* (Sciochetti et al., 1999, 2001). SMC enrichment was largely unaffected in cells lacking RTP or the two DNA translocases (Figures 1B and S1C). In cells lacking *dif* or XerC, SMC enrichment was reduced in regions near *parS*, but the extent of enrichment was largely unchanged (Figure S1C). SMC enrichment in the $\Delta xerD$ mutant was even more reduced near *parS* and appeared to modestly extend beyond the terminus region (Figure 1B, black caret). DNA juxtaposition, as assayed by Hi-C, was also altered in the $\Delta xerD$ mutant, proceeding modestly but reproducibly beyond the terminus region (Figure S1D). Furthermore, we observed a reduction in DNA juxtaposition in the terminus region in wild-type cells that was largely absent in the $\Delta xerD$ mutant (Figure S1E). These results prompted us to explore a potential role for XerCD/*dif* in preventing SMC rings from traveling beyond the terminus.

Consistent with previous *in vitro* studies (Blakely et al., 1993; Sciochetti et al., 2001), ChIP-seq with a XerC-GFP fusion strain identified a single XerC enrichment peak centered at *dif* (Figure 2A) that was dependent on XerD and *dif* (Figures 2A and S2C). In contrast, a XerD-GFP fusion not only had an enrichment peak at *dif* but also had five additional peaks in the terminus region (Figure 2B). Similar results were obtained with XerC and XerD fusions to a Protein C (PrC) epitope (Griffin et al., 1981; Zheng et al., 2018) (Figures S2A and S2B). Although XerD enrichment at *dif* depended on XerC and *dif*, enrichment at the other five sites was independent of these factors (Figures 2B and S2D). Four of these XerD-specific enrichment peaks spanned a 316 kb region and were present in all ChIP-seq experiments, while the fifth was variable and always weaker than the other four (Figures 2B, 2C, and S2B). Statistical analysis indicates that XerD's enrichment at *XDS1–4* sites was significant in all three replicates; enrichment at *XDS5* was significant in two of three replicates (Figure S2E). Motif discovery algorithms from the MEME suite (<http://meme-suite.org/>) identified a putative binding site (named *XDS*, for XerD binding site) that was present within each enrichment peak and absent from the rest of the genome (Figure 2D). These *XDS* sites contain the XerD binding motif at *dif* adjacent to a sequence that does not resemble the XerC binding motif (Figure 2D). Deleting the *XDS1* sequence resulted in the loss of the XerD enrichment peak at 1,717 kb, and inserting *XDS1* at 2,540 kb generated a new peak at this ectopic position (Figure 2C).

The XerD-XDS interaction was further analyzed in *E. coli* via a reporter ($P_{XDS1}\text{-}lacZ$) in which *XDS1* was inserted between the -10 and -35 elements of a synthetic promoter (Cho and Bernhardt, 2013) such that transcription of *lacZ* is repressed if a protein binds to *XDS1* (Figure 2E). *B. subtilis* XerD was expressed under IPTG control, and LacZ production was analyzed on LB agar plates containing X-gal. In the absence of IPTG, the *E. coli* colonies were blue (Figure 2E); in its presence, the col-

onies were white. In contrast, expression of *E. coli* XerD or *B. subtilis* XerC using identical promoter fusions failed to repress transcription (Figure 2E). We conclude that XerD binds directly to the *XDS* sites and appears to do so without additional co-factors.

B. subtilis cells lacking XerC or *dif* grow similarly to the wild-type (Figure 3A), and their chromosomes (called nucleoids) have relatively homogeneous morphologies (Sciochetti et al., 1999) (Figures 3B, 3C, S2G, and S3). In contrast, cells lacking XerD are growth defective, and their nucleoids are heterogeneous in size and appear distended (Lemon et al., 2001; Sciochetti et al., 1999) (Figures 3A–3C, S2G, and S3). Importantly, the growth defect of $\Delta xerD$ was not suppressed by deletions of *xerC* (Cornet et al., 1997) (Figure S2H) or *recA* (Blakely et al., 1993; Kuempel et al., 1991) (Figure S2I), consistent with the idea that XerD has a second function outside of dimer resolution. To investigate whether these phenotypic differences relate to XerD bound to *XDS* sites, we analyzed a strain in which all five sites were deleted (*XDS* $\Delta 5$). The growth and nucleoid morphologies of the mutant cells were similar to those lacking XerC or *dif* (Figures 3A–3C, S2G, and S3). However, when the *XDS* deletions were combined with $\Delta xerC$, Δdif , or $\Delta xerD$, the cells largely resembled the $\Delta xerD$ mutant (Figures 3A–3C, S2G, and S3). Analysis of the replication origins revealed that the distended nucleoids in the $\Delta xerD$ single mutant and the double mutants that lack the *XDS* sites contained multiple origins (Figure 3D). As the DNA replication profiles of these strains were similar to wild-type (Figure S2F), these findings indicate that chromosome segregation is impaired in the mutants. Thus, in addition to its role in dimer resolution, XerD has a second function in chromosome segregation that requires its XerD-specific binding sites.

Close examination of the SMC ChIP-seq profile in the strain harboring the -117° *parS* suggests that XerD's second function is related to condensin. Five statistically significant SMC enrichment peaks in the terminus region coincided with XerD enrichment peaks at *dif* and the four strong *XDS* sites (Figures 4A and S4A–S4C). At higher resolution, the XerD and SMC enrichment peaks were superimposable (Figures 4C and S4D). Furthermore, SMC enrichment at the *XDS* sites required XerD and *XDS* (Figures 4A–4C, S4D, and S4E), while enrichment at *dif* required XerC, XerD, and *dif* (Figures 4A and S4E). Importantly, all five SMC enrichment peaks were also present in wild-type and a strain harboring ectopic *parS* sites at -153° or -94° (Figure S4A). In contrast, there was no correlation between SMC enrichment in the terminus region and the Ter sites bound by RTP (Figure S4B), and in strains lacking RTP or the DNA translocases SpollIE and SftA, the SMC enrichment peaks at *XDS* sites were intact (Figure 4B). Finally, the overall ChIP-seq profile in the strain lacking all five *XDS* sites and harboring a *parS* site at -117° was similar to the profile in the $\Delta xerD$ mutant (Figures 4A and 4B). Altogether, these data suggest that SMC complexes are acted upon by XerD bound to *XDS* in the terminus region.

XerD, in complex with XerC, not only resolves chromosome dimers at *dif* sites but has also been found to help resolve catenated chromosomes in *E. coli* (Grainge et al., 2007; Ip et al., 2003; Shimokawa et al., 2013). Inefficient or impaired removal of these topological barriers could explain why DNA juxtaposition extended so modestly beyond the terminus region in the $\Delta xerD$ mutant (Figure S1D, black carets). To circumvent potential topological

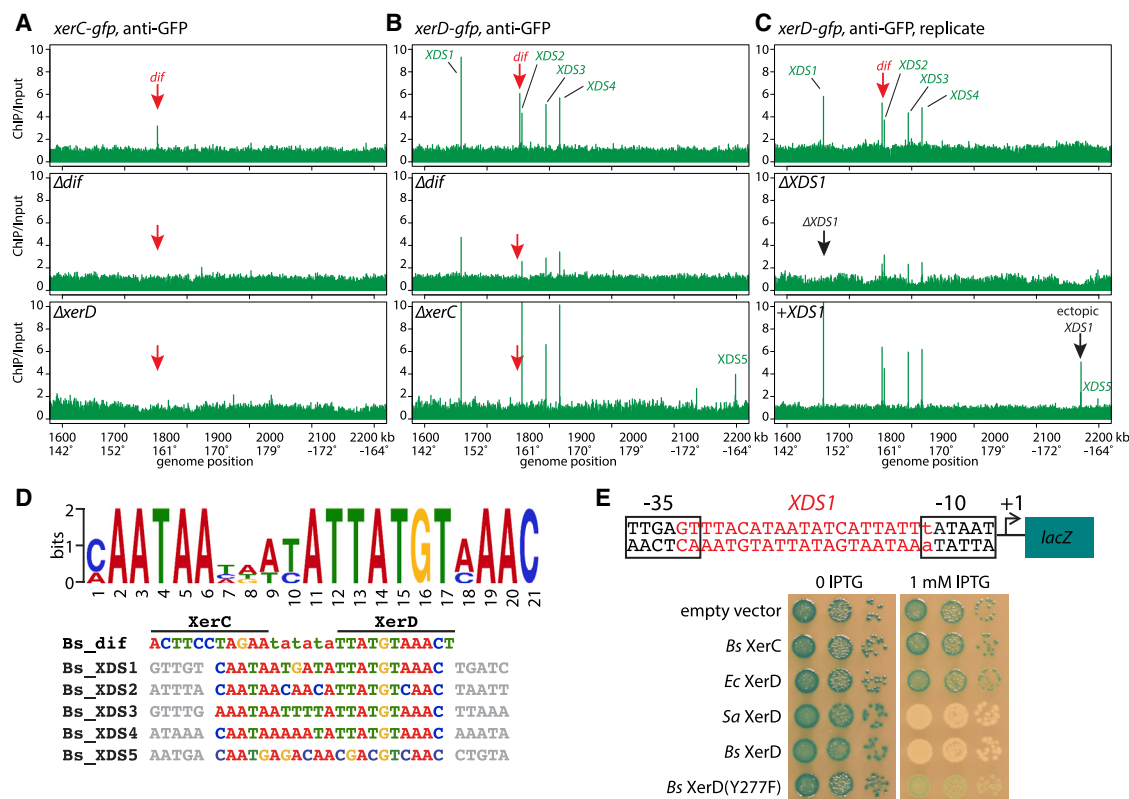


Figure 2. Identification of XerD-specific binding sites at replication terminus

(A) Enrichment profiles from anti-GFP ChIP-seq performed in strains containing *xerC-gfp* in otherwise wild-type (WT) (top), Δ *dif* (middle), or Δ *xerD* (bottom) strains. Sequencing reads from ChIP and input samples were normalized to the total number of reads. The ChIP enrichment (ChIP/Input) is shown in 1 kb bins. The position of the *dif* site is indicated by a red arrow.

(B) Enrichment profiles from anti-GFP ChIP-seq performed in strains containing *xerD-gfp* in otherwise WT (top), Δ *dif* (middle), or Δ *xerC* (bottom) strains. XerD-GFP is enriched at four sites (XDS1–4) in addition to *dif*. A fifth XerD binding site (XDS5) is present in a subset of experiments (B, bottom; C, bottom; Figure S2B). XDS sites do not appear to have a specific orientation. XDS1 (+strand), *dif* (+strand), XDS2 (–strand), XDS3 (+strand), XDS4 (–strand), XDS5 (–strand). Quantitative analysis of ChIP-seq experiments can be found in Figure S2E.

(C) Enrichment profiles from anti-GFP ChIP-seq plots in strains containing *xerD-gfp* in otherwise WT (top, biological replicate to the top panel of B), a strain with XDS1 deleted (middle), and a strain with XDS1 inserted at 2,540 kb (bottom).

(D) Top: logo of XerD binding site generated with XDS1–4. Bottom: the five XerD binding sites compared with *B. subtilis* *dif* with indicated XerC and XerD binding motifs.

(E) XerD binds to XDS1 in *E. coli*. The indicated proteins from *B. subtilis* (*Bs*), *E. coli* (*Ec*), and *S. aureus* (*Sa*) were expressed under IPTG control. White colonies on LB(X-gal+IPTG) are indicative of protein binding to XDS1 and repression of *lacZ* transcription. XerD* is a catalytic XerD mutant (Y277F).

impediments to SMC movement, we investigated whether recruitment of XerD to an ectopic position blocks DNA juxtaposition and SMC translocation. Arrays of XDS sites were inserted at -109° in a strain with a single *parS* site at -94° , 175 kb away. DNA interaction frequencies from the -94° *parS* to the -109° XDS array (and its juxtaposed locus at -84°) were similar to those in a strain without an array (Figures 5A–5C, S5A, and S5B). However, interactions beyond these positions were reduced to ~50% with an array of 4 XDS sites and to background level with an array of 12 sites (Figures 5B, 5C, S5A, and S5B). We note that the XDS arrays also generated a chromosome interaction boundary that was SMC and XerD dependent (Figures S5C and S5F), suggesting a distinct role for SMC complexes in short-range interactions along the chromosome (Lioy et al., 2018). SMC enrichment as assayed by ChIP-seq was largely restricted to the region between -84° and -109° (Figures 5B and 5C). Importantly, the block to DNA

juxtaposition and SMC enrichment required XerD but not XerC (Figure S5F). Similar results were obtained when the (XDS)12 array was inserted at -80° (Figure S6A) or in a strain that contained a *parS* site at -59° and an (XDS)12 array at -109° (Figures S6B and S6C). An even more dramatic loss of DNA juxtaposition was observed when the (XDS)12 array was inserted at $+26^\circ$ or -19° in a strain harboring a native *parS* site at -1° (Figures 5E and S5D). Importantly, DNA juxtaposition and SMC enrichment were not affected by TetR-CFP fusions bound to an array of 48 *tetO* operators (Figure S5E) and marker frequency analysis indicates that the (XDS)12 array did not impair DNA replication (Figure S5G). We note that strains with one or two ectopic XDS sites did not impair SMC enrichment (Figure S6D), perhaps because of the large step size predicted for these translocases (see Discussion) (Davidson et al., 2019; Ganji et al., 2018; Kim et al., 2019; Terakawa et al., 2017).

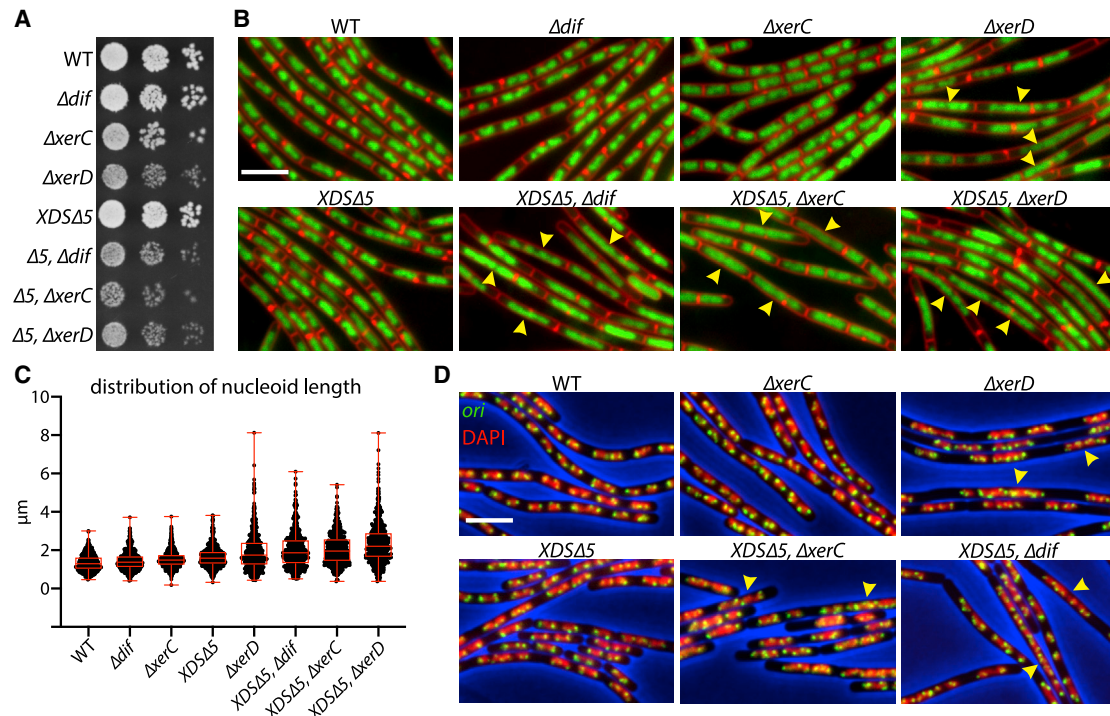


Figure 3. Cells lacking XerD have defects in chromosome segregation

(A) 10-fold serial dilutions of the indicated strains spotted on LB agar.

(B) Representative images of the indicated strains. DAPI-stained DNA (green) and FM4-64-stained membranes (red) are shown. Scale bar indicates 4 μ m. Distended nucleoids are highlighted (yellow carets). Larger fields can be found in Figure S3.

(C) Quantitative analysis of nucleoid length. Boxplot showing the mean, quartiles, minimum, and maximum of nucleoid length of the indicated strains plotted with Prism (GraphPad). Individual data points are plotted in black. Numbers are shown in Figure S2G. Two-tailed t test was performed for each pair of strains. Except for two pairs ($\Delta xerD$ versus $XDS\Delta 5\Delta dif$ and $XDS\Delta 5\Delta dif$ versus $XDS\Delta 5\Delta xerC$), all the pairs have a significant difference in the distribution of nucleoid length ($p < 0.05$).

(D) Merged images of replication origins (green) labeled with GFP-ParB and DAPI-stained DNA (red). Unsegregated nucleoids are highlighted (yellow carets).

The data presented thus far are consistent with a model in which XerD bound to XDS sites functions to unload rather than stall SMC complexes. The SMC enrichment peaks at XDS sites in the terminus region were narrow (Figures 4C and S4D) and lacked a shoulder that would have resulted from a “pileup” of stalled condensin complexes. Furthermore, if XerD stalled SMC complexes at the XDS array, the -109° locus harboring the array would have interacted with regions beyond its juxtaposed position at -84° . Similarly, SMC would have been enriched beyond the -84° site (Figure 5C). We contrast the Hi-C and ChIP-seq data from strains harboring an ectopic XDS array to those from a strain in which a chromosomal locus was artificially tethered to the cytoplasmic membrane to stall SMC translocation (Figure 5D). A TetR fusion to the Tsr membrane-anchoring domain (Tsr-TetR-YFP) (Magnan et al., 2015) bound to an array of 120 tetO operators prevented DNA juxtaposition beyond the tetO array at -122° . However, the -122° locus interacted with a ~ 330 kb region on the juxtaposed DNA (Figure 5D, green arrow). Similarly, SMC was highly enriched at the tetO array and strongly depleted beyond it, while on the juxtaposed DNA there was no sharp boundary of depletion (Figure 5D, bottom). Thus, these data provide further support for the idea that XerD functions as a site-specific unloader of SMC complexes.

We took advantage of the ability to site-specifically unload condensin to investigate whether SMC complexes, once loaded, translocate autonomously and unidirectionally down the chromosome arms or whether directed movement requires a point source of newly loaded complexes. Using a strain harboring a single origin-proximal parS site at -1° , (XDS)12 arrays at $+26^\circ$ and -19° , and an IPTG-inducible allele of XerD as the sole source of the protein, we performed Hi-C on cells grown in the absence of IPTG and at 5 min intervals after its addition. Prior to IPTG addition, the interactions between the left and right arm were similar to a strain harboring a -1° parS site (Figures 5E and 5G). After addition of IPTG, interactions were progressively lost starting from the terminus-proximal side of the XDS arrays (Figure 5G), while DNA juxtaposition remained unchanged between the origin-proximal parS and the arrays. Quantification of the loss of DNA juxtaposition indicates that the rate of “unzipping” (51 ± 5 kb/min) was similar to the ~ 50 kb/min rate of zip-up using an IPTG-inducible allele of ParB, the condensin loader (Wang et al., 2017, 2018). Thus, once loaded, SMC complexes translocate directionally and autonomously along DNA (Figure 5F).

S. aureus possesses the genes encoding the SMC complex, ParB, and origin-proximal parS sites (Chan et al., 2020; Kuroda et al., 2001; Livny et al., 2007) as well as *xerCD* and *dif*. To

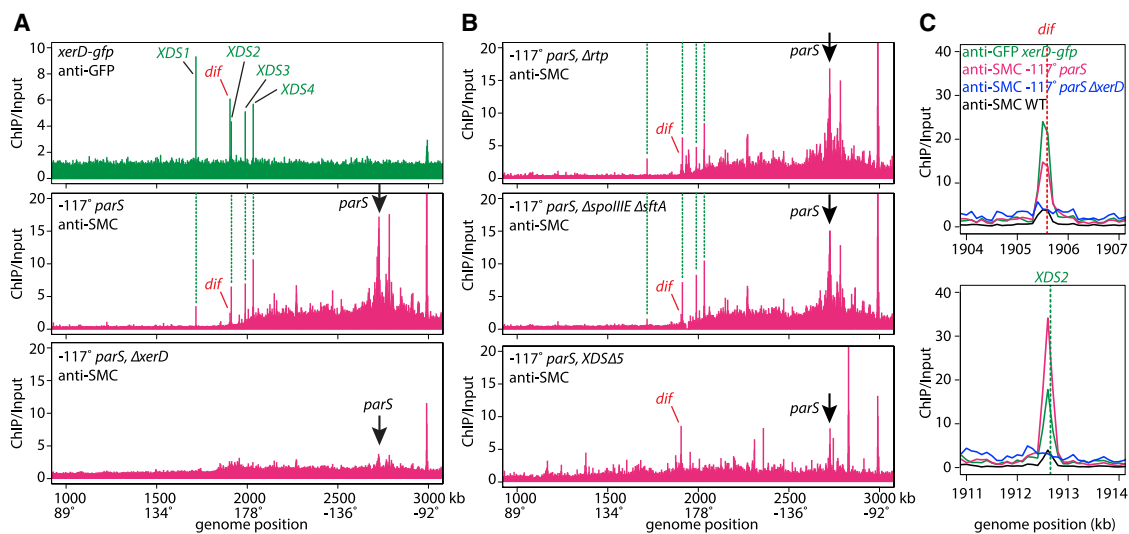


Figure 4. SMC is enriched at XerD binding sites

(A) Top: anti-GFP ChIP-seq performed in a strain containing *xerD-gfp*. Middle and bottom: anti-SMC ChIP-seq from a strain containing a single *parS* site at -117° in a WT or $\Delta xerD$ background. Green dotted lines and black arrows indicate the positions of the *XDS* and *parS* sites, respectively. Biological replicates and quantitative analysis of ChIP-seq experiments can be found in Figures S4A and S4C.

(B) Anti-SMC ChIP-seq performed in a strain containing -117° *parS* site in *Δxtp*, *ΔspolIIIEΔsftA*, or lacking the five XerD binding sites (*XDS15*).

(C) The *dif* and *XDS2* regions at higher resolution. Anti-GFP ChIP-seq from a *xerD-gfp* strain (green), anti-SMC ChIP-seq in WT (black), a strain containing a -117° *parS* site (magenta), or $\Delta xerD$ (blue). The other *XDS* sites can be found in Figure S4D. Normalized ChIP enrichment (ChIP/Input) is plotted in 100 bp bins.

investigate whether the role of XerD in SMC unloading was conserved in this bacterium, we generated a XerD-His6 fusion and performed ChIP-seq. Five XerD enrichment peaks in addition to *dif* were identified in the terminus region (Figure 6A). A putative XerD binding site was present within each peak that resembled the *XDS* sites found in *B. subtilis* (Figure 6B), and expression of *S. aureus* XerD in *E. coli* was sufficient to inhibit $P_{XDS1}-lacZ$ expression (Figure 2E). To establish whether XerD bound to these sites could promote condensin unloading, we introduced the *(XDS)12* array at 40° in the *S. aureus* genome and analyzed the conformation of the chromosome by Hi-C. In wild-type *S. aureus*, the left and right chromosome arms interacted along their length, and these interactions were dependent on ParB (Figure 6C). Importantly, the *XDS* array blocked DNA juxtaposition beyond its insertion site at 40°. Thus, XerD/XDS-dependent unloading of SMC complexes at the replication terminus is likely to be a conserved feature of bacterial chromosome biology.

DISCUSSION

Altogether our data provide an integrated view of bacterial chromosome segregation in which two broadly conserved factors that play central roles in chromosome segregation at the origin and terminus have second functions in loading and unloading SMC complexes that travel between them (Figure 7). Specifically, work in several bacteria indicates that ParB proteins bound to origin-proximal *parS* sites are acted upon by ParA to segregate newly replicated origins toward opposite cell poles (Fogel and Waldor, 2006; Harms et al., 2013; Lim et al., 2014; Shebelut et al., 2010; Toro et al., 2008; Wang et al., 2014a). Origin resolution and chromosome segregation are facilitated by the action of SMC complexes that

are themselves loaded at the origin by ParB/*parS* nucleoprotein complexes (Gruber and Errington, 2009; Sullivan et al., 2009; Wilhelm et al., 2015). Once loaded, these complexes translocate down the left and right chromosome arms in the wake of the replisomes (Marbouy et al., 2015; Minnen et al., 2016; Wang et al., 2015). During transit, the SMC complexes tether the left and right arms together, drawing sister chromatids in on themselves and away from each other (Wang et al., 2017). This directed movement likely facilitates Topoisomerase IV-mediated resolution of pre-catenanes (Bürmann and Gruber, 2015) generated by the rotation of the replisome, a consequence of the torsional strain of unwinding the DNA helix (Peter et al., 1998). When the replisome reaches the terminus, dimeric and interlinked chromosomes are resolved by XerC-XerD bound to *dif* (Blakely et al., 1993; Sciochetti et al., 2001) and by Topoisomerase IV (Zechiedrich and Cozzarelli, 1995). Meanwhile, XerD bound to *XDS* sites in the terminus region unloads SMC complexes liberating them to re-load at the replication origin. The symmetry and economy in the resolution and segregation of replicating *B. subtilis* chromosomes described here is likely to be broadly conserved among bacteria.

We note that in strains with one or two ectopic *XDS* sites, SMC enrichment along the chromosome arms was largely unaffected (Figure S6D). It is unclear why the presence of one or two sites was not sufficient to unload SMC complexes and why robust unloading required an array with 4 *XDS* sites. If the movement of SMC complexes involves large step sizes (Davidson et al., 2019; Ganji et al., 2018; Kim et al., 2019; Terakawa et al., 2017), then it is possible that these translocating ATPases could bypass XerD bound to a single *XDS*, as has been suggested for cohesin and CTCF at topologically associated domain boundaries (Hansen et al., 2017). In the case of the native *XDS* sites,

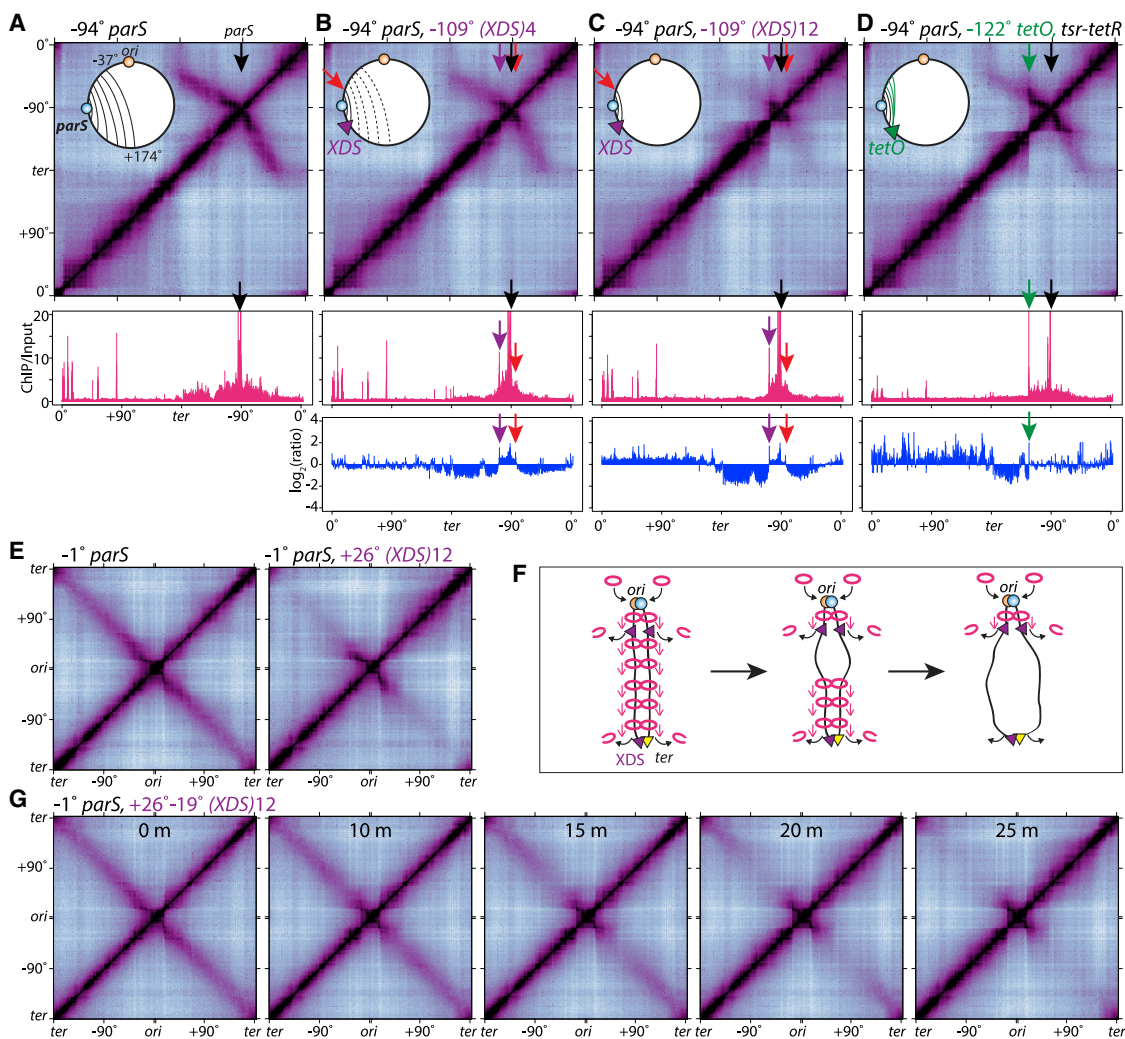


Figure 5. XerD is required for condensin unloading

(A–C) Normalized Hi-C contact maps of strains containing a single *parS* at -94° (A) and arrays of 4 (B) or 12 (C) *XDS* sites inserted at -109° . Quantitative analysis of Hi-C data can be found in Figures S5A and S5B. Anti-SMC ChIP-seq profiles (magenta) are shown underneath the Hi-C maps. The ratio of ChIP-seq relative to -94° *parS* strain is plotted in blue. Black and purple arrows show the positions of *parS* and the *XDS* array. The position (-84°) juxtaposed with the -109° *XDS* array is shown (red arrow). SMC enrichment is reduced beyond the *XDS* array and the juxtaposed position, 2-fold in the strain containing *(XDS)4* and 4-fold in *(XDS)12*. The loss of SMC enrichment from both arms is contrasted to the non-specific loss of SMC on the origin-proximal side of *parS* observed in Figure S1B. (D) Hi-C and ChIP-seq plots of a strain containing a *parS* site at -94° *parS* site, (*tetO*) 120 at -122° (green arrow), and *tsr-tetR-yfp*. Expression of *tsr-tetR-yfp* was induced (1 mM IPTG) for 1 h. Green arrow on the Hi-C map points to the interactions between the -122° locus and a ~ 330 kb region on the juxtaposed DNA. (E) Hi-C contact maps of a strain containing -1° *parS*, and *(XDS)12* at $+26^\circ$. The Hi-C maps are oriented with the origin at the center of the axes. (F and G) Unzipping of juxtaposed DNA upon XerD induction in a strain with *(XDS)12* arrays at -19° and $+26^\circ$. Origin-centered Hi-C maps before and after IPTG addition. Time (in minutes) is shown.

once *B. subtilis* condensin complexes reach the terminus with no more DNA to translocate along the stalled complexes would have multiple opportunities to encounter XerD bound to the limited number of sites in the terminus region.

The data presented here demonstrate that SMC complexes can be removed from the genome in a site-specific manner. Although we cannot rule out the possibility that XerD recruits a factor that unloads SMC, we favor a model in which XerD itself functions as the site-specific unloader. The mechanism by which XerD catalyzes SMC removal from the chromosome is currently unknown. We note that an XerD catalytic point mutant (Y277F)

(Cornet et al., 1997) was able to prevent DNA juxtaposition and SMC translocation beyond an ectopic *XDS* array, even though it bound *XDS* sites less efficiently than wild-type XerD (Figures 2E, S5A, S5B, and S7). These data argue against a model in which XerD unloads condensin by cutting the chromosome and “unthreading” topologically loaded condensin rings. Instead, we favor the idea that XerD allosterically controls ring opening through its interaction with one of the proteins in the complex. A central challenge for the future is to define in molecular terms how ParB/*parS* loads SMC complexes onto DNA and how XerD/*XDS* catalyzes their removal.

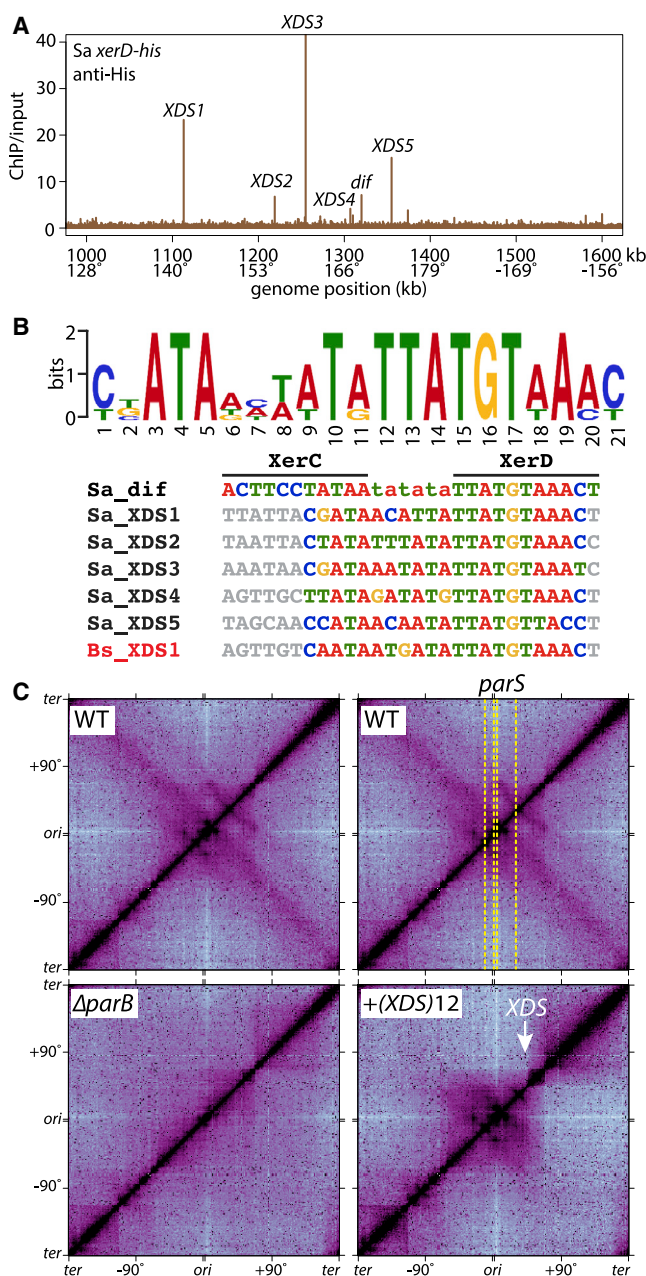


Figure 6. ParB and XerD perform similar functions in *S. aureus*

(A) Anti-His ChIP-seq performed in a *xerD-his6* *S. aureus* strain.
(B) Logo of *S. aureus* XerD binding sites. Sequences of the five XerD binding sites compared with *S. aureus* dif and *B. subtilis* XDS1 are shown. XerC and XerD binding motifs at dif are highlighted.
(C) Normalized Hi-C contact maps of *S. aureus* WT, Δ parB, and a strain with the *B. subtilis* (XDS)12 array at +40°. Yellow dotted lines show the positions of parS sites. White arrow indicates the position of the XDS array.

Limitations of study

The results presented in this study indicate that XerD bound to XDS sites functions in unloading SMC complexes when they reach the terminus. Although we favor the idea the XerD is itself the unloader, it is possible that XerD recruits an unknown factor to the terminus

region that catalyzes SMC removal. Biochemical reconstitution using purified components will be required to unambiguously establish whether XerD possesses condensin unloading activity.

STAR★METHODS

Detailed methods are provided in the online version of this paper and include the following:

- **KEY RESOURCES TABLE**
- **RESOURCE AVAILABILITY**
 - Lead contact
 - Materials availability
 - Data and code availability
- **EXPERIMENTAL MODEL AND SUBJECT DETAILS**
 - *Bacillus subtilis* strains and growth
- **METHOD DETAILS**
 - Hi-C
 - ChIP-seq
 - ChIP-seq analysis
 - Biological replicates
 - Microscopy
 - Plasmid construction
 - Strain construction (*B. subtilis*)
 - Strain construction (*E. coli*)
 - Strain construction (*S. aureus*)
- **QUANTIFICATION AND STATISTICAL ANALYSIS**
 - Analysis of nucleoid length
 - Analysis of XerC and XerD ChIP-Seq peaks
 - Analysis of SMC ChIP-Seq peaks at XDS sites

SUPPLEMENTAL INFORMATION

Supplemental Information can be found online at <https://doi.org/10.1016/j.molcel.2020.12.027>.

ACKNOWLEDGMENTS

Hi-C and ChIP-seq data were deposited in the Gene Expression Omnibus (GSE144742). We thank members of the Wang, Rudner, and Bernhardt labs for stimulating discussions and support; the Indiana University Center for Genomics and Bioinformatics and the Tufts University Core Facility for assistance with high throughput sequencing; A. Grossman for anti-SMC antibodies; T. Bernhardt, H. Cho, and T. Pang for plasmids and strains; A. Kruse and S. Zeng for anti-PrC antibodies; and J. Livny for *in silico* investigation of XDS sites. Support for this work comes from startup funds from Indiana University (X.W.) and National Institutes of Health grants GM086466 and GM073831 (D.Z.R.). H.B.B. was supported by a Natural Sciences and Engineering Research Council of Canada Post-Graduate Fellowship (doctoral).

AUTHOR CONTRIBUTIONS

X.W. and D.Z.R. designed the study. X.W. and X.K. constructed strains and performed ChIP-seq, whole-genome sequencing, microscopy experiments, and analyses. X.W. and Z.R. performed Hi-C experiments and analyses. H.B.B. analyzed Hi-C and ChIP-seq data and performed statistical analyses. P.P. constructed strains and assisted with Hi-C experiments. X.W. and D.Z.R. wrote the manuscript.

DECLARATION OF INTERESTS

The authors declare no competing interests.

Molecular Cell

Article

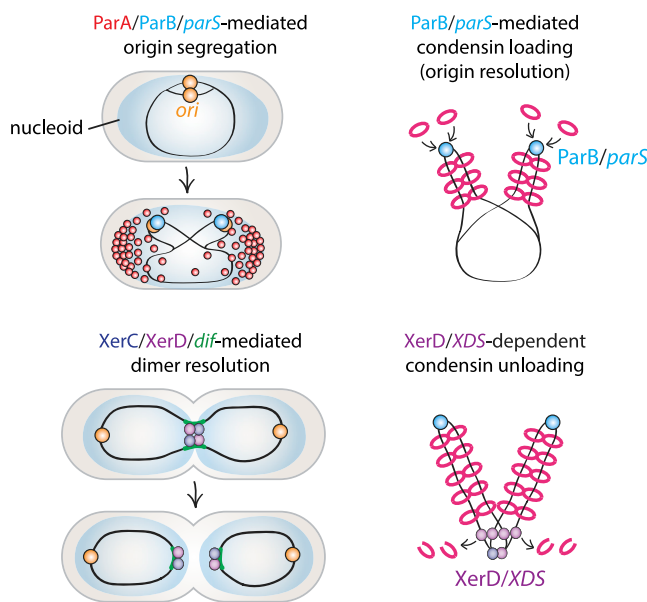


Figure 7. Schematic model

Bacterial SMC complexes are loaded onto and unloaded from chromosomes by conserved factors that function in origin segregation and terminus resolution. ParB/parS nucleoprotein complexes (light blue circles) adjacent to newly replicated origins (orange circles) are segregated toward opposite cell poles by ParA (red circles) bound non-specifically throughout the nucleoid. XerC and XerD (dark blue and purple circles) resolve dimeric chromosomes at *dif* sites (green). SMC complexes (magenta rings) are loaded at newly replicated origins by ParB/parS and then travel down the left and right arms while tethering them together. Loop extrusion draws newly replicated sisters in on themselves and away from each other and facilitates the removal of interlinks by Topoisomerase IV (not shown). When the tethered rings reach the terminus, they are unloaded by XerD bound to XDS sites (purple).

Received: June 8, 2020

Revised: October 11, 2020

Accepted: December 14, 2020

Published: January 19, 2021

SUPPORTING CITATIONS

The following references appear in the supplemental information: Griffith and Grossman, (2008); Guyer et al. (1981); Nair et al. (2011); Wang et al. (2014b).

REFERENCES

- Badrinarayanan, A., Reyes-Lamothe, R., Uphoff, S., Leake, M.C., and Sherratt, D.J. (2012). In vivo architecture and action of bacterial structural maintenance of chromosome proteins. *Science* 338, 528–531.
- Badrinarayanan, A., Le, T.B., and Laub, M.T. (2015). Bacterial chromosome organization and segregation. *Annu. Rev. Cell Dev. Biol.* 31, 171–199.
- Bernhardt, T.G., and de Boer, P.A. (2004). Screening for synthetic lethal mutants in *Escherichia coli* and identification of EnvC (YibP) as a periplasmic septal ring factor with murein hydrolase activity. *Mol. Microbiol.* 52, 1255–1269.
- Blakely, G., May, G., McCulloch, R., Arciszewska, L.K., Burke, M., Lovett, S.T., and Sherratt, D.J. (1993). Two related recombinases are required for site-specific recombination at *dif* and *cer* in *E. coli* K12. *Cell* 75, 351–361.
- Böhm, K., Giacomelli, G., Schmidt, A., Imhof, A., Koszul, R., Marbouy, M., and Bramkamp, M. (2020). Chromosome organization by a conserved condensin system in the actinobacterium *Corynebacterium glutamicum*. *Nat. Commun.* 11, 1485.
- Brandão, H.B., Paul, P., van den Berg, A.A., Rudner, D.Z., Wang, X., and Mirny, L.A. (2019). RNA polymerases as moving barriers to condensin loop extrusion. *Proc. Natl. Acad. Sci. U S A* 116, 20489–20499.
- Bürmann, F., and Gruber, S. (2015). SMC condensin: promoting cohesion of replicon arms. *Nat. Struct. Mol. Biol.* 22, 653–655.
- Chan, H., Söderström, B., and Skoglund, U. (2020). SpoJ and SMC are required for normal chromosome segregation in *Staphylococcus aureus*. *MicrobiologyOpen* 9, e999.
- Cho, H., and Bernhardt, T.G. (2013). Identification of the SlmA active site responsible for blocking bacterial cytokinetic ring assembly over the chromosome. *PLoS Genet.* 9, e1003304.
- Cornet, F., Hallet, B., and Sherratt, D.J. (1997). Xer recombination in *Escherichia coli*. Site-specific DNA topoisomerase activity of the XerC and XerD recombinases. *J. Biol. Chem.* 272, 21927–21931.
- Crobat, E., Rousseau, P., Fournes, F., and Cornet, F. (2014). The FtsK family of DNA translocases finds the ends of circles. *J. Mol. Microbiol. Biotechnol.* 24, 396–408.
- Davidson, I.F., Bauer, B., Goetz, D., Tang, W., Wutz, G., and Peters, J.M. (2019). DNA loop extrusion by human cohesin. *Science* 366, 1338–1345.
- Duggin, I.G., Wake, R.G., Bell, S.D., and Hill, T.M. (2008). The replication fork trap and termination of chromosome replication. *Mol. Microbiol.* 70, 1323–1333.
- Fogel, M.A., and Waldor, M.K. (2006). A dynamic, mitotic-like mechanism for bacterial chromosome segregation. *Genes Dev.* 20, 3269–3282.
- Ganji, M., Shaltiel, I.A., Bisht, S., Kim, E., Kalichava, A., Haering, C.H., and Dekker, C. (2018). Real-time imaging of DNA loop extrusion by condensin. *Science* 360, 102–105.
- Grainge, I., Bregu, M., Vazquez, M., Sivanathan, V., Ip, S.C., and Sherratt, D.J. (2007). Unlinking chromosome catenanes in vivo by site-specific recombination. *EMBO J.* 26, 4228–4238.
- Griffin, J.H., Evatt, B., Zimmerman, T.S., Kleiss, A.J., and Wideman, C. (1981). Deficiency of protein C in congenital thrombotic disease. *J. Clin. Invest.* 68, 1370–1373.
- Griffith, K.L., and Grossman, A.D. (2008). Inducible protein degradation in *Bacillus subtilis* using heterologous peptide tags and adaptor proteins to target substrates to the protease ClpXP. *Mol. Microbiol.* 70, 1012–1025.
- Gruber, S., and Errington, J. (2009). Recruitment of condensin to replication origin regions by ParB/SpoJ promotes chromosome segregation in *B. subtilis*. *Cell* 137, 685–696.
- Guyer, M.S., Reed, R.R., Steitz, J.A., and Low, K.B. (1981). Identification of a sex-factor-affinity site in *E. coli* as gamma delta. *Cold Spring Harb. Symp. Quant. Biol.* 45, 135–140.
- Haldimann, A., and Wanner, B.L. (2001). Conditional-replication, integration, excision, and retrieval plasmid-host systems for gene structure-function studies of bacteria. *J. Bacteriol.* 183, 6384–6393.
- Hansen, A.S., Pustova, I., Cattoglio, C., Tjian, R., and Darzacq, X. (2017). CTCF and cohesin regulate chromatin loop stability with distinct dynamics. *eLife* 6, e25776.
- Harms, A., Treuner-Lange, A., Schumacher, D., and Søgaard-Andersen, L. (2013). Tracking of chromosome and replisome dynamics in *Myxococcus xanthus* reveals a novel chromosome arrangement. *PLoS Genet.* 9, e1003802.
- Harris, C.R., Millman, K.J., van der Walt, S.J., Gommers, R., Virtanen, P., Cournapeau, D., Wieser, E., Taylor, J., Berg, S., Smith, N.J., et al. (2020). Array programming with NumPy. *Nature* 585, 357–362.
- Harwood, C.R., and Cutting, S.M. (1990). *Molecular Biological Methods for Bacillus* (New York: John Wiley).
- Hassler, M., Shaltiel, I.A., and Haering, C.H. (2018). Towards a unified model of SMC complex function. *Curr. Biol.* 28, R1266–R1281.
- Herbert, S., Ziebandt, A.K., Ohlsen, K., Schäfer, T., Hecker, M., Albrecht, D., Novick, R., and Götz, F. (2010). Repair of global regulators in

- Staphylococcus aureus 8325 and comparative analysis with other clinical isolates. *Infect. Immun.* 78, 2877–2889.
- Hirano, T. (2016). Condensin-based chromosome organization from bacteria to vertebrates. *Cell* 164, 847–857.
- Imakaev, M., Fudenberg, G., McCord, R.P., Naumova, N., Goloborodko, A., Lajoie, B.R., Dekker, J., and Mirny, L.A. (2012). Iterative correction of Hi-C data reveals hallmarks of chromosome organization. *Nat. Methods* 9, 999–1003.
- Ip, S.C., Bregu, M., Barre, F.X., and Sherratt, D.J. (2003). Decatenation of DNA circles by FtsK-dependent Xer site-specific recombination. *EMBO J.* 22, 6399–6407.
- Jensen, R.B. (2006). Analysis of the terminus region of the Caulobacter crescentus chromosome and identification of the dif site. *J. Bacteriol.* 188, 6016–6019.
- Johnson, J.E., Lackner, L.L., Hale, C.A., and de Boer, P.A. (2004). ZipA is required for targeting of DMinC/DicB, but not DMinC/MinD, complexes to septal ring assemblies in Escherichia coli. *J. Bacteriol.* 186, 2418–2429.
- Kaimer, C., Schenk, K., and Graumann, P.L. (2011). Two DNA translocases synergistically affect chromosome dimer resolution in Bacillus subtilis. *J. Bacteriol.* 193, 1334–1340.
- Kim, Y., Shi, Z., Zhang, H., Finkelstein, I.J., and Yu, H. (2019). Human cohesin compacts DNA by loop extrusion. *Science* 366, 1345–1349.
- Koo, B.M., Kritikos, G., Farelli, J.D., Todor, H., Tong, K., Kimsey, H., Wapinski, I., Galardini, M., Cabal, A., Peters, J.M., et al. (2017). Construction and analysis of two genome-scale deletion libraries for Bacillus subtilis. *Cell Syst.* 4, 291–305.e7.
- Kuempel, P.L., Henson, J.M., Dircks, L., Tecklenburg, M., and Lim, D.F. (1991). dif, a recA-independent recombination site in the terminus region of the chromosome of Escherichia coli. *New Biol.* 3, 799–811.
- Kunst, F., Ogasawara, N., Moszer, I., Albertini, A.M., Alloni, G., Azevedo, V., Bertero, M.G., Bessières, P., Bolotin, A., Borchert, S., et al. (1997). The complete genome sequence of the gram-positive bacterium Bacillus subtilis. *Nature* 390, 249–256.
- Kuroda, M., Ohta, T., Uchiyama, I., Baba, T., Yuzawa, H., Kobayashi, I., Cui, L., Oguchi, A., Aoki, K., Nagai, Y., et al. (2001). Whole genome sequencing of methicillin-resistant Staphylococcus aureus. *Lancet* 357, 1225–1240.
- Landgraf, D., Okumus, B., Chien, P., Baker, T.A., and Paulsson, J. (2012). Segregation of molecules at cell division reveals native protein localization. *Nat. Methods* 9, 480–482.
- Lau, I.F., Filipe, S.R., Søballe, B., Økstad, O.-A., Barre, F.-X., and Sherratt, D.J. (2003). Spatial and temporal organization of replicating Escherichia coli chromosomes. *Mol. Microbiol.* 49, 731–743.
- Lemon, K.P., Kurtser, I., and Grossman, A.D. (2001). Effects of replication termination mutants on chromosome partitioning in Bacillus subtilis. *Proc. Natl. Acad. Sci. U.S.A.* 98, 212–217.
- Lesterlin, C., Barre, F.X., and Cornet, F. (2004). Genetic recombination and the cell cycle: what we have learned from chromosome dimers. *Mol. Microbiol.* 54, 1151–1160.
- Lim, H.C., Surovtsev, I.V., Beltran, B.G., Huang, F., Bewersdorf, J., and Jacobs-Wagner, C. (2014). Evidence for a DNA-relay mechanism in ParABS-mediated chromosome segregation. *eLife* 3, e02758.
- Lindow, J.C., Kuwano, M., Moriya, S., and Grossman, A.D. (2002). Subcellular localization of the Bacillus subtilis structural maintenance of chromosomes (SMC) protein. *Mol. Microbiol.* 46, 997–1009.
- Liou, V.S., Cournac, A., Marbouty, M., Duigou, S., Mozziconacci, J., Espéli, O., Boccard, F., and Koszul, R. (2018). Multiscale structuring of the *E. coli* chromosome by nucleoid-associated and condensin proteins. *Cell* 172, 771–783.e18.
- Livny, J., Yamaichi, Y., and Waldor, M.K. (2007). Distribution of centromere-like parS sites in bacteria: insights from comparative genomics. *J. Bacteriol.* 189, 8693–8703.
- Magnan, D., Joshi, M.C., Barker, A.K., Visser, B.J., and Bates, D. (2015). DNA replication initiation is blocked by a distant chromosome-membrane attachment. *Curr. Biol.* 25, 2143–2149.
- Mäkelä, J., and Sherratt, D.J. (2020). Organization of the *Escherichia coli* chromosome by a MukBEF axial core. *Mol. Cell* 78, 250–260.e5.
- Marbouty, M., Le Gall, A., Cattoni, D.I., Cournac, A., Koh, A., Fiche, J.B., Mozziconacci, J., Murray, H., Koszul, R., and Nollmann, M. (2015). Condensin- and replication-mediated bacterial chromosome folding and origin condensation revealed by Hi-C and super-resolution imaging. *Mol. Cell* 59, 588–602.
- Marko, J.F. (2009). Linking topology of tethered polymer rings with applications to chromosome segregation and estimation of the knotting length. *Phys. Rev. E Stat. Nonlin. Soft Matter Phys.* 79, 051905.
- Marko, J.F., De Los Rios, P., Barducci, A., and Gruber, S. (2019). DNA-segment-capture model for loop extrusion by structural maintenance of chromosome (SMC) protein complexes. *Nucleic Acids Res.* 47, 6956–6972.
- Meeske, A.J., Sham, L.T., Kimsey, H., Koo, B.M., Gross, C.A., Bernhardt, T.G., and Rudner, D.Z. (2015). MurJ and a novel lipid II flippase are required for cell wall biogenesis in *Bacillus subtilis*. *Proc. Natl. Acad. Sci. U.S.A.* 112, 6437–6442.
- Midonet, C., and Barre, F.X. (2014). Xer site-specific recombination: promoting vertical and horizontal transmission of genetic information. *Microbiol. Spectr.* 2 (6).
- Minnen, A., Attaiech, L., Thon, M., Gruber, S., and Veening, J.W. (2011). SMC is recruited to oriC by ParB and promotes chromosome segregation in *Streptococcus pneumoniae*. *Mol. Microbiol.* 81, 676–688.
- Minnen, A., Bürmann, F., Wilhelm, L., Anchimiuk, A., Diebold-Durand, M.L., and Gruber, S. (2016). Control of Smc coiled coil architecture by the ATPase heads facilitates targeting to chromosomal ParB/parS and release onto flanking DNA. *Cell Rep.* 14, 2003–2016.
- Nair, D., Memmi, G., Hernandez, D., Bard, J., Beaume, M., Gill, S., Francois, P., and Cheung, A.L. (2011). Whole-genome sequencing of *Staphylococcus aureus* strain RN4220, a key laboratory strain used in virulence research, identifies mutations that affect not only virulence factors but also the fitness of the strain. *J. Bacteriol.* 193, 2332–2335.
- Nolivos, S., Upton, A.L., Badrinarayanan, A., Müller, J., Zawadzka, K., Wiktor, J., Gill, A., Arciszewska, L., Nicolas, E., and Sherratt, D. (2016). MatP regulates the coordinated action of topoisomerase IV and MukBEF in chromosome segregation. *Nat. Commun.* 7, 10466.
- Pang, T., Wang, X., Lim, H.C., Bernhardt, T.G., and Rudner, D.Z. (2017). The nucleoid occlusion factor Noc controls DNA replication initiation in *Staphylococcus aureus*. *PLoS Genet.* 13, e1006908.
- Peter, B.J., Ullsperger, C., Hiasa, H., Marians, K.J., and Cozzarelli, N.R. (1998). The structure of supercoiled intermediates in DNA replication. *Cell* 94, 819–827.
- Rajasekar, K.V., Baker, R., Fisher, G.L.M., Bolla, J.R., Mäkelä, J., Tang, M., Zawadzka, K., Koczy, O., Wagner, F., Robinson, C.V., et al. (2019). Dynamic architecture of the *Escherichia coli* structural maintenance of chromosomes (SMC) complex, MukBEF. *Nucleic Acids Res.* 47, 9696–9707.
- Reyes-Lamothe, R., Nicolas, E., and Sherratt, D.J. (2012). Chromosome replication and segregation in bacteria. *Annu. Rev. Genet.* 46, 121–143.
- Rudner, D.Z., Fawcett, P., and Losick, R. (1999). A family of membrane-embedded metalloproteases involved in regulated proteolysis of membrane-associated transcription factors. *Proc. Natl. Acad. Sci. U.S.A.* 96, 14765–14770.
- Schroeder, J.W., and Simmons, L.A. (2013). Complete genome sequence of *Bacillus subtilis* strain PY79. *Genome Announc.* 1, e01085-13.
- Sciochetti, S.A., Piggot, P.J., Sherratt, D.J., and Blakely, G. (1999). The ripX locus of *Bacillus subtilis* encodes a site-specific recombinase involved in proper chromosome partitioning. *J. Bacteriol.* 181, 6053–6062.
- Sciochetti, S.A., Piggot, P.J., and Blakely, G.W. (2001). Identification and characterization of the dif Site from *Bacillus subtilis*. *J. Bacteriol.* 183, 1058–1068.

Molecular Cell

Article



- Shebelut, C.W., Guberman, J.M., van Teeffelen, S., Yakhnina, A.A., and Gitai, Z. (2010). Caulobacter chromosome segregation is an ordered multistep process. *Proc. Natl. Acad. Sci. U S A* **107**, 14194–14198.
- Sherratt, D.J., Arciszewska, L.K., Crozat, E., Graham, J.E., and Grainge, I. (2010). The Escherichia coli DNA translocase FtsK. *Biochem. Soc. Trans.* **38**, 395–398.
- Shimokawa, K., Ishihara, K., Grainge, I., Sherratt, D.J., and Vazquez, M. (2013). FtsK-dependent XerCD-dif recombination unlinks replication catenanes in a stepwise manner. *Proc. Natl. Acad. Sci. U S A* **110**, 20906–20911.
- Sullivan, N.L., Marquis, K.A., and Rudner, D.Z. (2009). Recruitment of SMC by ParB-parS organizes the origin region and promotes efficient chromosome segregation. *Cell* **137**, 697–707.
- Terakawa, T., Bisht, S., Eeftens, J.M., Dekker, C., Haering, C.H., and Greene, E.C. (2017). The condensin complex is a mechanochemical motor that translocates along DNA. *Science* **358**, 672–676.
- Toro, E., Hong, S.H., McAdams, H.H., and Shapiro, L. (2008). Caulobacter requires a dedicated mechanism to initiate chromosome segregation. *Proc. Natl. Acad. Sci. U S A* **105**, 15435–15440.
- Tran, N.T., Laub, M.T., and Le, T.B.K. (2017). SMC progressively aligns chromosomal arms in Caulobacter crescentus but is antagonized by convergent transcription. *Cell Rep.* **20**, 2057–2071.
- Uhlmann, F. (2016). SMC complexes: from DNA to chromosomes. *Nat. Rev. Mol. Cell Biol.* **17**, 399–412.
- Val, M.E., Kennedy, S.P., El Karoui, M., Bonné, L., Chevalier, F., and Barre, F.X. (2008). FtsK-dependent dimer resolution on multiple chromosomes in the pathogen Vibrio cholerae. *PLoS Genet.* **4**, e1000201.
- Virtanen, P., Gommers, R., Oliphant, T.E., Haberland, M., Reddy, T., Cournapeau, D., Burovski, E., Peterson, P., Weckesser, W., Bright, J., et al.; SciPy 1.0 Contributors (2020). SciPy 1.0: fundamental algorithms for scientific computing in Python. *Nat. Methods* **17**, 261–272.
- Wang, X., Montero Llopis, P., and Rudner, D.Z. (2014a). *Bacillus subtilis* chromosome organization oscillates between two distinct patterns. *Proc. Natl. Acad. Sci. U S A* **111**, 12877–12882.
- Wang, X., Tang, O.W., Riley, E.P., and Rudner, D.Z. (2014b). The SMC condensin complex is required for origin segregation in *Bacillus subtilis*. *Curr. Biol.* **24**, 287–292.
- Wang, X., Le, T.B., Lajoie, B.R., Dekker, J., Laub, M.T., and Rudner, D.Z. (2015). Condensin promotes the juxtaposition of DNA flanking its loading site in *Bacillus subtilis*. *Genes Dev.* **29**, 1661–1675.
- Wang, X., Brandão, H.B., Le, T.B., Laub, M.T., and Rudner, D.Z. (2017). *Bacillus subtilis* SMC complexes juxtapose chromosome arms as they travel from origin to terminus. *Science* **355**, 524–527.
- Wang, X., Hughes, A.C., Brandão, H.B., Walker, B., Lierz, C., Cochran, J.C., Oakley, M.G., Kruse, A.C., and Rudner, D.Z. (2018). In vivo evidence for ATPase-dependent DNA translocation by the *Bacillus subtilis* SMC condensin complex. *Mol. Cell* **71**, 841–847.e5.
- Wilhelm, L., Bürmann, F., Minnen, A., Shin, H.-C., Toseland, C.P., Oh, B.-H., and Gruber, S. (2015). SMC condensin entraps chromosomal DNA by an ATP hydrolysis dependent loading mechanism in *Bacillus subtilis*. *eLife* **10**, e06659.
- Yatskevich, S., Rhodes, J., and Nasmyth, K. (2019). Organization of chromosomal DNA by SMC complexes. *Annu. Rev. Genet.* **53**, 445–482.
- Youngman, P.J., Perkins, J.B., and Losick, R. (1983). Genetic transposition and insertional mutagenesis in *Bacillus subtilis* with *Streptococcus faecalis* transposon Tn917. *Proc. Natl. Acad. Sci. U S A* **80**, 2305–2309.
- Zechiedrich, E.L., and Cozzarelli, N.R. (1995). Roles of topoisomerase IV and DNA gyrase in DNA unlinking during replication in *Escherichia coli*. *Genes Dev.* **9**, 2859–2869.
- Zhang, Y., Liu, T., Meyer, C.A., Eeckhoute, J., Johnson, D.S., Bernstein, B.E., Nusbaum, C., Myers, R.M., Brown, M., Li, W., and Liu, X.S. (2008). Model-based analysis of ChIP-Seq (MACS). *Genome Biol.* **9**, R137.
- Zheng, S., Sham, L.T., Rubino, F.A., Brock, K.P., Robins, W.P., Mekalanos, J.J., Marks, D.S., Bernhardt, T.G., and Kruse, A.C. (2018). Structure and mutagenic analysis of the lipid II flippase MurJ from *Escherichia coli*. *Proc. Natl. Acad. Sci. U S A* **115**, 6709–6714.

STAR★METHODS

KEY RESOURCES TABLE

REAGENT or RESOURCE	SOURCE	IDENTIFIER
Antibodies		
Anti-SMC polyclonal rabbit antibody	(Lindow et al., 2002)	N/A
Anti-GFP polyclonal rabbit antibody, affinity purified	(Rudner et al., 1999)	N/A
Anti-His tag antibody	GenScript	Cat # A00186-100; RRID:AB_914704
Anti-PrC	(Zheng et al., 2018)	N/A
Chemicals, peptides, and recombinant proteins		
Formaldehyde 37%	Sigma	Cat # F8775
Ready-Lyse Lysozyme	Epicenter	Cat # R1802M
HindIII	NEB	Cat # R0104M
Klenow	NEB	Cat # M0210L
Biotin-14-dATP	ThermoFisher	Cat # 19524016
T4 DNA ligase	NEB	Cat # M0202M
Proteinase K	NEB	Cat # P8107S
T4 DNA Polymerase	NEB	Cat # M0203L
X-gal	VWR	Cat # 97061-648
IPTG	Dot Scientific	Cat # DS102125
nProtein-A Sepharose 4 Fast Flow	GE Healthcare	Cat # 45002981
nProtein-G Sepharose 4 Fast Flow	GE Healthcare	Cat # 45000116
RNase A	Promega	Cat # R7973
DAPI	ThermoFisher	Cat # D1306
FM4-64	ThermoFisher	Cat # 12518100A3
Critical commercial assays		
NEBNext Ultra II DNA Library Prep Kit	NEB	Cat # E7645S
Deposited data		
Raw and analyzed Hi-C, ChIP-seq, WGS data	This paper	GEO: GSE144742; See Table S4
Published Hi-C	(Brandão et al., 2019; Wang et al., 2015)	See Table S4
Published Hi-C and ChIP-seq	(Wang et al., 2017)	See Table S4
Published ChIP-seq	(Brandão et al., 2019; Wang et al., 2015)	See Table S4
Original Data	Mendeley Data	https://doi.org/10.17632/8zdhwm28nc.1
Experimental models: organisms/strains		
<i>Bacillus subtilis</i> strains, see Table S1	N/A	N/A
<i>Escherichia coli</i> strains, see Table S1	N/A	N/A
<i>Staphylococcus aureus</i> strains, see Table S1	N/A	N/A
Oligonucleotides		
See Table S3	N/A	N/A
Recombinant DNA		
See Table S2	N/A	N/A
Software and algorithms		
Hiclib	(Imakaev et al., 2012)	https://github.com/mirnylab/hiclib-legacy
MATLAB 8.5 (R2015)	(Wang et al., 2017)	https://www.mathworks.com/

(Continued on next page)

Continued

REAGENT or RESOURCE	SOURCE	IDENTIFIER
MetaMorph	Molecular Devices	https://www.moleculardevices.com/
Numpy 1.18.1	(Harris et al., 2020)	https://numpy.org/
Pandas 1.0.1	The pandas development team	https://zenodo.org/record/3644238
Python 3.7.6	N/A	https://www.python.org/
Prism	GraphPad	https://www.graphpad.com/scientific-software/prism/
R	N/A	https://www.r-project.org
Scipy 1.4.1	(Virtanen et al., 2020)	https://www.scipy.org/

RESOURCE AVAILABILITY

Lead contact

Further information and requests for resources and reagents should be directed to and will be fulfilled by the Lead Contact Xindan Wang (xindan@indiana.edu).

Materials availability

Plasmids and strains generated in this study are available from the Lead Contact with a completed Materials Transfer Agreement.

Data and code availability

Unprocessed microscopy images are available at Mendeley data: <https://doi.org/10.17632/8zdhwm28nc.1>. The accession number for Hi-C data (raw and analyzed) is GEO: GSE144742. The scripts for the Hi-C and statistical analyses are available from the Lead Contact upon request without restriction.

EXPERIMENTAL MODEL AND SUBJECT DETAILS

Bacillus subtilis strains and growth

Bacillus subtilis strains were derived from the prototrophic strain PY79 (Youngman et al., 1983). Cells were grown in defined rich medium (CH) (Harwood and Cutting, 1990) at 37°C with aeration. *Staphylococcus aureus* strains were derived from HG003 (Herbert et al., 2010) and were grown in tryptic soy broth (TSB) at 37°C with aeration. Lists of strains, plasmids, oligonucleotides and Next Generation Sequencing samples can be found in Tables S1, S2, S3, and S4.

METHOD DETAILS

Hi-C

The detailed Hi-C procedure for *B. subtilis* was previously described (Wang et al., 2015). Briefly, 5x10⁷ cells were crosslinked with 3% formaldehyde at room temperature for 30 min then quenched with 125 mM glycine. Cells were lysed using Ready-Lyse Lysozyme (Epicenter, R1802M) followed by 0.5% SDS treatment. Solubilized chromatin was digested with HindIII for 2 hr at 37°C. The cleaved ends were filled in with Klenow and Biotin-14-dATP, dGTP, dCTP, dTTP. The products were ligated in dilute reactions with T4 DNA ligase overnight at 16°C. Crosslinks were reversed at 65°C overnight in the presence proteinase K. The DNA was then extracted twice with phenol/chloroform/isoamylalcohol (25:24:1) (PCI), precipitated with ethanol, and resuspended in 20 µl of QIAGEN EB buffer. Biotin from non-ligated ends was removed using T4 polymerase (4 hr at 20°C) followed by extraction with PCI. The DNA was then sheared by sonication for 12 min with 20% amplitude using a Qsonica Q800R2 water bath sonicator. The sheared DNA was used for library preparation with the NEBNext UltraII kit (E7645) according to the manufacturer's instructions for end repair, adaptor ligation, and size selection. Biotinylated DNA fragments were purified using 10 µl streptavidin beads. 5 µl DNA-bound beads were used for PCR in a 50 µl reaction for 14 cycles. PCR products were purified using Ampure beads and sequenced at the Indiana University Center for Genomics and Bioinformatics using NextSeq 550 or at the Tufts University Core facility using HiSeq 2500. Paired-end sequencing reads were mapped to the genome of *B. subtilis* PY79 (NCBI Reference Sequence NC_022898.1) using the same pipeline described previously (Wang et al., 2015). The *B. subtilis* PY79 genome was first divided into 404 10-kb bins. Subsequent analysis and visualization was done using R scripts. The genetic loci marked by degree (°) were calculated using the PY79 genome, which results in a slight shift from data published using *B. subtilis* 168 genomic coordinates.

Hi-C procedure for *S. aureus* was similar to that of *B. subtilis* described above, except that cells were lysed using 3 µL Ready-Lyse Lysozyme (Epicenter, R1802M) and 5 µL of 10 mg/ml lysostaphin. Paired-end sequencing reads were mapped to the genome of *S. aureus* NCTC8325 genome (NCBI NC_007795.1), which was divided into 2822 10-kb bins.

ChIP-seq

Chromatin immunoprecipitation (ChIP) for *B. subtilis* was performed as described previously (Wang et al., 2015). Briefly, cells were crosslinked using 3% formaldehyde for 30 min at room temperature and then quenched, washed, and lysed. Chromosomal DNA was sheared to an average size of 250 bp by sonication using a Qsonica Q800R2 water bath sonicator. The lysate was then incubated overnight at 4°C with appropriate antibodies. When anti-SMC (Lindow et al., 2002) or anti-GFP (Rudner et al., 1999) antibodies were used, lysates were incubated with Protein A Sepharose (GE HealthCare) for 1 h at 4°C. When Protein C antibodies (Zheng et al., 2018) were used, lysates were included with Protein G Sepharose (GE HealthCare). After washes and elution, the immunoprecipitate was incubated at 65°C overnight to reverse the crosslinks. The DNA was further treated with RNaseA, Proteinase K, extracted with PCI, resuspended in 50 µL EB and used for library preparation with the NEBNext UltraII kit (E7645) and sequenced using the Illumina MiSeq or NextSeq550 platforms. The sequencing reads were aligned to the *B. subtilis* PY79 genome (NCBI NC_022898.1) using CLC Genomics Workbench (CLC Bio, QIAGEN), and subsequently normalized, plotted and analyzed using R scripts.

ChIP for *S. aureus* was performed similar *B. subtilis*, except that 1) cells were lysed using 3 µL Ready-Lyse Lysozyme (Epicenter, R1802M) and 80 µL of 10 mg/ml lysostaphin; 2) anti-His antibodies (Genescrypt 10498-106) and Protein G-Sepharose (GE HealthCare) were used; and 3) sequencing reads were mapped to the genome of *S. aureus* NCTC8325 (NCBI NC_007795.1).

ChIP-seq analysis

Sequencing reads from ChIP and input samples were normalized to the total number of reads. The ChIP enrichment (ChIP/Input) was plotted. After excluding enriched regions containing highly transcribed genes which are enriched in every ChIP-seq experiment we have done regardless of the strain or antibodies used (Wang et al., 2017), we manually identified peaks with greater than 3-fold ChIP/input enrichment. For XerC-GFP (Figure 2A) and XerC-PrC (Figure S2A), we identified a single peak at *dif*, which was statistically significant in both samples (Figure S2E). For two replicates of XerD-GFP (Figures 2B and 2C) and one sample of XerD-PrC (Figure S2B), in addition to the *dif* site, we identified four sites (XDS1-4) statistically significant in all three samples and a fifth site (XDS5) significant in two out of the three samples (Figure S2E). Details on the statistical tests can be found in the legend of Figure S2E.

We used the 4 strong sites (XDS1-4) to compute the logo using MEME and identified a 21 nt consensus sequence which contains 15 consensus nucleotide positions and 6 degenerate positions (Figure 2D). Bioinformatically, if we fix the consensus positions but allow the 6 degenerate positions to have random sequences, only XDS1-4 are observed. If we additionally allow one mismatch in the consensus locations, we identified one more site near the replication origin. But there was no enrichment peak at this position in any of the 7 relevant samples shown in Figures 2 and S2. If we allow two mismatches at consensus locations, we observed 43 additional sites throughout the genome. The XDS5 site has 4 mismatches at the consensus locations and failed to make to this cut off.

Biological replicates

For the ChIP-seq analysis of XerD binding sites, two biological replicates were performed using XerD-GFP and one replicate using XerD-PrC. Control ChIP-seq experiments with XerC-GFP and XerC-PrC were each performed one time. These replicates are included in Figures 2B, 2C, S2A, and S2B with quantitative analysis in Figure S2E.

For the ChIP-Seq analysis of SMC enrichment along the chromosome arms and the specific enrichment at XDS sites, two biological replicates were performed in a strain in which *parS* was inserted at -117° and two replicates in a strain in which *parS* was inserted at -94°. These replicates are included in Figure S4A.

For Hi-C experiments, two biological replicates were performed in strains containing -117°*parS* in the presence and absence of *xerD*. These can be found Figure S1D. The replicates were highly reproducible. Most of the other strains analyzed in this study by Hi-C were performed only once. However, the conclusions were drawn from Hi-C data obtained using complementary strains. For example, the effect of XDS sites on DNA juxtaposition was analyzed in strains in which *parS* was present at several distinct locations in the genome and in strains in which the XDS array was inserted at different genomic positions. All of these experiments were internally consistent providing support for our conclusions but do not allow for a traditional quantitative analysis. Figures in which different ectopic *parS* sites were analyzed by Hi-C include Figures 1, 5, S1, S5, and S6. Figures in which different ectopic XDS sites were analyzed by Hi-C include Figures 5, S5, and S6.

Microscopy

Fluorescence microscopy was performed on a Nikon Ti2E microscope equipped with Plan Apo 100x/1.4NA phase contrast oil objective and an sCMOS camera. Cells were immobilized using 2% agarose pads containing growth media. Membranes were stained with FM4-64 (Molecular Probes) at 3 µg/ml. DNA was stained with DAPI at 2 µg/ml. Images were cropped and adjusted using MetaMorph software (Molecular Devices). Final figures were prepared in Adobe Illustrator.

Plasmid construction

pWX118L [*yrvN* (-122°)::tetO120 (*cat*)] was generated by inserting tetO120 (liberated with NheI and HindIII from pLAU39 CGSC#: 12311 (Lau et al., 2003)) into pWX109 between NheI and HindIII. pWX109 [*yrvN*::*cat*] is an ectopic integration vector for double crossover insertions into the *yrvN* locus (X.W. and D.Z.R., unpublished data). The genetic location by degrees (°) in this study is calculated using the PY79 genome sequence (CP006881) (Schroeder and Simmons, 2013), which is slightly different from our previous publications using *B. subtilis* 168 genome coordinates (NC_000964) (Kunst et al., 1997).

pWX618 [*pelB::Psoj (optRBS) mgfpmut3-spo0J (ΔparS) (cat)*] was constructed in a 3-way ligation to insert *mgfpmut3* with an optimal ribosome binding site (*optRBS*) (amplified using oWX706 and oWX674 from pDHL580 (Landgraf et al., 2012) and digested with HindIII and Xhol) and *spo0J (ΔparS)* (excised from pKM256 using Xhol and BamHI) into pKM170 [*pelB::Psoj (cat)*] (Sullivan et al., 2009) between HindIII and BamHI. *spo0J (ΔparS)* has 7 synonymous changes in the 16-base *parS* site in the *spo0J* (Sullivan et al., 2009). *parB* was named *spo0J* in *B. subtilis*.

pWX702 [*yvbj::Pspank (optRBS) tsr-tetR-yfp (erm)*] was generated in a 3-way ligation to insert *tsr* (Magnan et al., 2015) with an optimal ribosome binding site (*optRBS*) (amplified using oWX1429 and oWX1430 from *E. coli* MG1655 genome and digested with HindIII and XbaI) and *tetR-yfp* (amplified using oWX1431 and oWX1432 from pWX187 and digested with XbaI and XmaI) into pMS44 [*yvbj::Pspank (erm)*] (D.Z.R., unpublished data) between HindIII and XmaI. The construct was sequenced using oWX486, oWX487, oWX669, oWX1434, oWX1435.

pWX720 [*yvbj::Pspank (optRBS) xerD (cat)*] was generated by inserting *xerD* with an optimal ribosome binding site (*optRBS*) (amplified using oWX1645 and oWX1646 from *B. subtilis* PY79 genome and digested with XmaI and NheI) into pER134 [*yvbj::Pspank (cat)*] (D.Z.R., unpublished data) between XmaI and NheI. The construct was sequenced using oWX486 and odr829.

pWX725 [*Ptet (optRBS) Sa xerD-his6 (cat)*] was generated by inserting *S. aureus* *xerD* with an optimal ribosome binding site (*optRBS*) (amplified using oWX1706 and oWX1707 from *S. aureus* HG003 (Herbert et al., 2010) genome and digested with KpnI and XmaI) into pTP171 (Pang et al., 2017) between KpnI and XmaI. pTP171 is an *S. aureus* integration plasmid that contains *Ptet (optRBS)* *Bs noc-his6 cat*. The construct was sequenced using oWX1710 and oWX1711.

pWX726 [*(XDS)12 (loxP-kan-loxP)*] was generated by an isothermal assembly reaction containing 2 PCR products: 1) *(XDS)12 loxP-kan-loxP* (amplified using oWX1563 and oWX438 from the genomic DNA of BWX3805 (see strain construction); 2) pTP171 (Pang et al., 2017) amplified using oWX1712 and oWX1713. The construct was sequenced using oTP263 and oML83.

pWX730 [*attλ cat Plac::Bs xerD*] was generated by an isothermal assembly reaction containing 2 PCR products: 1) *Bs xerD* (amplified using oWX1721 and oWX1722 from PY79 genomic DNA; 2) pHC886 [*attλ cat Plac* empty vector] (H. Cho and T. G. Bernhardt, personal communication) amplified using oWX1397 and oWX1398. The construct was sequenced using oWX1403 and oWX1404.

pWX731 [*attλ cat Plac::Bs xerD (Y277F)*] was generated by an isothermal assembly reaction containing 2 PCR products: 1) *Bs xerD Y277F* (amplified using oWX1721 and oWX1722 from genomic DNA of BWX3896 (see strain construction); 2) pHC886 [*attλ cat Plac* empty vector] (H. Cho and T. G. Bernhardt, personal communication) amplified using oWX1397 and oWX1398. The construct was sequenced using oWX1403 and oWX1404.

pWX732 [*attλ cat Plac::Bs xerC*] was generated by an isothermal assembly reaction containing 2 PCR products: 1) *Bs xerC* (amplified using oWX1723 and oWX1724 from PY79 genomic DNA; 2) pHC886 [*attλ cat Plac* empty vector] (H. Cho and T. G. Bernhardt, personal communication) amplified using oWX1397 and oWX1398. The construct was sequenced using oWX1403 and oWX1404.

pWX737 [*attλ cat Plac::Ec xerD*] was generated by an isothermal assembly reaction containing 2 PCR products: 1) *Ec xerD* (amplified using oWX1725 and oWX1726 from *E. coli* MG1655 genomic DNA; 2) pHC886 [*attλ cat Plac* empty vector] (H. Cho and T. G. Bernhardt, personal communication) amplified using oWX1397 and oWX1398. The construct was sequenced using oWX1403 and oWX1404.

pWX738 [*attλ cat Plac::Sa xerD*] was generated by an isothermal assembly reaction containing 2 PCR products: 1) *Sa xerD* (amplified using oWX1727 and oWX1728 from *E. coli* MG1655 genomic DNA; 2) pHC886 [*attλ cat Plac* empty vector] (H. Cho and T. G. Bernhardt, personal communication) amplified using oWX1397 and oWX1398. The construct was sequenced using oWX1403 and oWX1404.

Strain construction (*B. subtilis*)

The *Δrtp*, *ΔspolIIIE*, *ΔsftA*, *ΔxerC* and *ΔxerD* mutants marked with *loxP-erm-loxP* are derived from the *Bacillus subtilis* knockout collection (Koo et al., 2017). Genomic DNA of these knockout strains was extracted and backcrossed with PY79 twice. Each deletion was confirmed by PCR using oKO0 (within the erythromycin resistance cassette) and an upstream gene-specific primer: for *rtp* (oWX1186), *xerC* (oWX1448), *xerD* (oWX1187), *spolIIIE* (oWX1175), and *sftA* (oWX1176). In some cases, the *loxP-erm-loxP* cassette was removed using a *cre* expressing plasmid pDR244 (Meeske et al., 2015).

Δdif loxP-kan-loxP (BWX3510) or loxP-spec-loxP (BWX3508)

The *dif* site (ACTTCCTAGAATATATTATGTAACT) was deleted by directly transforming an isothermal assembly product to PY79. The isothermal assembly reaction contained 3 PCR products: 1) the region upstream of *dif* (amplified from PY79 genomic DNA using oWX1377 and oWX1378); 2) *loxP-kan-loxP* cassette or *loxP-spec-loxP* cassette (amplified from pWX470 or pWX466 using universal primers oWX438 and oWX439) and 3) the region downstream of *dif* (amplified from PY79 genomic DNA using primers oWX1379 and oWX1380). The transformants were amplified and sequenced using oWX1381 and oWX1382.

+58° parS loxP-kan-loxP (BWX3388)

The +4° *parS* sequence (TGTTACACGTGAAACA) was inserted at +58° (in the intergenic region between *yeaB* and *yeaC*). An isothermal assembly product was directly transformed to *parS49* (BWX3212) (Wang et al., 2015), which has all the 9 *parS* sites deleted from the *B. subtilis* genome. The isothermal assembly reaction contained 3 PCR products: 1) a region containing *yeaB* (amplified from PY79 genomic DNA using oWX1309 and oWX1310); 2) *loxP-kan-loxP* cassette flanked by the +4° *parS* sequence (amplified from pWX470 using universal primers oWX1241 and oWX438) and 3) a region containing *yeaC* (amplified from PY79 genomic DNA using primers oWX1311 and oWX1312). The transformants were amplified and sequenced using oWX1313 and oWX1314.

+117°parS loxP-kan-loxP (BWX3389).

The +4° *parS* sequence (TGTACACGTGAAACA) was inserted at +117° (in the intergenic region between *ykcC* and *htrA*). An isothermal assembly product was directly transformed to *parS49* (BWX3212) (Wang et al., 2015). The isothermal assembly reaction contained 3 PCR products: 1) a region containing *ykcC* gene (amplified from PY79 genomic DNA using oWX1315 and oWX1316); 2) *loxP-kan-loxP* cassette flanked by the +4° *parS* sequence (amplified from pWX470 using universal primers oWX1241 and oWX438) and 3) a region containing *htrA* (amplified from PY79 genomic DNA using primers oWX1317 and oWX1318). The transformants were amplified and sequenced using oWX1319 and oWX1320.

+153°parS loxP-kan-loxP (BWX3391).

The +4° *parS* sequence (TGTACACGTGAAACA) was inserted at +153° (in the intergenic region between *ymfJ* and *ymfK*). An isothermal assembly product was directly transformed to *parS49* (BWX3212) (Wang et al., 2015). The isothermal assembly reaction contained 3 PCR products: 1) a region containing *ymfJ* gene (amplified from PY79 genomic DNA using oWX1321 and oWX1322); 2) *loxP-kan-loxP* cassette flanked by the +4° *parS* sequence (amplified from pWX470 using universal primers oWX1241 and oWX438) and 3) a region containing *ymfK* (amplified from PY79 genomic DNA using primers oWX1323 and oWX1324). The transformants were amplified and sequenced using oWX1325 and oWX1326.

ΔrecA loxP-spec-loxP (BWX3649).

The *recA* gene was deleted by directly transforming an isothermal assembly product to PY79. The isothermal assembly reaction contained 3 PCR products: 1) the region upstream of *recA* (amplified from PY79 genomic DNA using oWX1441 and oWX1442); 2) *loxP-spec-loxP* cassette (amplified from pWX466 using universal primers oWX438 and oWX439) and 3) the region downstream of *recA* (amplified from PY79 genomic DNA using primers oWX1443 and oWX1444). The transformants were amplified and sequenced using oWX1445 and oWX1446.

xerC-mgfpmut3 spec (BWX3653).

An isothermal assembly reaction containing the following 3 PCR products was directly transformed to PY79: 1) a region containing *xerC* and upstream region (amplified from PY79 genomic DNA using oWX1448 and oWX1449); 2) *mgfpmut3 spec* (amplified from pWX429 using oWX1385 and oWX1386); 3) a region downstream of *xerC* (amplified from PY79 genomic DNA using primers oWX1450 and oWX1451). The transformants were amplified using oWX1452 and oWX1453 and sequenced using oWX1452 and oML79. pWX429 contains *ycgO::PftsW lacI-mgfpmut3 spec* (X.W. and D.Z.R., unpublished data).

xerD-mgfpmut3 spec (BWX3655).

An isothermal assembly reaction containing the following 3 PCR products was directly transformed to PY79: 1) a region containing *xerD* and upstream region (amplified from PY79 genomic DNA using oWX1454 and oWX1455); 2) *mgfpmut3 spec* (amplified from pWX429 using oWX1385 and oWX1386); 3) the region downstream of *xerD* (amplified from PY79 genomic DNA using primers oWX1456 and oWX1457). The transformants were amplified using oWX1458 and oWX1459 and sequenced using oWX1458 and oML79.

yrdQ (2540kb)::XDS1 loxP-kan-loxP (BWX3724).

The *XDS1* site at 1717 kb was inserted between *yrdQ* and *yrdP* by transforming an isothermal assembly product to PY79. The isothermal assembly reaction contained 4 PCR products: 1) a region containing *yrdQ* (amplified from PY79 genomic DNA using oWX1504 and oWX1505); 2) *XDS1* at 1717 kb (amplified from the PY79 genomic DNA using oWX1502 and oWX1503) 3) *loxP-kan-loxP* cassette (amplified from pWX470 using universal primers oWX438 and oWX439); 4) a region containing *yrdP* (amplified from PY79 genomic DNA using primers oWX1506 and oWX1507). The transformants were amplified using oWX1508 and oWX1509, and sequenced using oWX1509.

-109° (XDS)4 loxP-spec-loxP (BWX3790).

The (XDS)4 array was synthesized at Integrated DNA Technologies (IDT) as gBlockWX06, which contains 50 bp regions centered at *XDS1* (1717kb), *XDS2* (1912kb), *XDS3* (1989kb), *XDS4* (2033kb), and two 20 bp sequences at the 5' end and 3' end of the construct for primer binding. This array was inserted at -109° (2802 kb) using an isothermal assembly reaction that contained 4 PCR products: 1) the region upstream of 2802 kb (amplified from PY79 genomic DNA using oWX1551 and oWX1552); 2) gBlockWX06; 3) *loxP-spec-loxP* cassette (amplified from pWX466 using universal primers oWX438 and oWX439); 4) the region downstream of 2802 kb (amplified from PY79 genomic DNA using primers oWX1553 and oWX1554). The transformants were amplified using oWX1555 and oWX1556, and sequenced using oWX1555.

-109° (XDS)12 loxP-kan-loxP (BWX3805).

The (XDS)12 array was synthesized at Integrated DNA Technologies (IDT) as gBlockWX07, which contains 30 bp regions centered at *XDS1* (1717kb), *XDS2* (1912kb), *XDS3* (1989kb) and *XDS4* (2033kb) repeated 3 times, and 20 bp unique spacer sequences between the XDS sites to reduce recombination. This fragment also contains two 20 bp sequences at the 5' end and 3' end for primer binding. This array was inserted at -109° (2802 kb) using an isothermal assembly reaction that contained 4 PCR products: 1) the region upstream of 2802 kb (amplified from PY79 genomic DNA using oWX1551 and oWX1552); 2) gBlockWX07; 3) *loxP-kan-loxP* cassette (amplified from pWX470 using universal primers oWX438 and oWX439); 4) the region downstream of 2802 kb (amplified from PY79 genomic DNA using primers oWX1553 and oWX1554). The transformants were amplified using oWX1555 and oWX1556, and sequenced using oWX1555. In some cases, the *loxP-kan-loxP* cassette was removed using a *cre* expressing plasmid pDR244 (Meeske et al., 2015).

-109° (XDS)12 loxP-spec-loxP (BWX3855).

This strain was constructed using the same method as BWX3805 except that a *loxP-spec-loxP* cassette was used (amplified from pWX466 using universal primers oWX438 and oWX439).

-80° (XDS)12 loxP-spec-loxP (BWX3858).

The (XDS)12 array was inserted at -80° (3128 kb) using an isothermal assembly reaction that contained 4 PCR products: 1) the region upstream of 3128 kb (amplified from PY79 genomic DNA using oWX1557 and oWX1558); 2) gBlockWX07; 3) *loxP-spec-loxP* cassette (amplified from pWX466 using universal primers oWX438 and oWX439); 4) the region downstream of 3128 kb (amplified from PY79 genomic DNA using primers oWX1559 and oWX1560). The transformants were amplified using oWX1561 and oWX1562, and sequenced using oWX1561.

-109° tetO48 cat (BWX3887).

An isothermal assembly reaction containing the following 3 PCR products was directly transformed to PY79: 1) the region upstream of 2802kb (amplified from PY79 genomic DNA using oWX1551 and oWX1552); 2) *tetO48 cat* cassette (amplified from pWX408 using oWX1591 and oWX1592); 3) the region downstream of 2802 kb (amplified from PY79 genomic DNA using primers oWX1553 and oWX1554). The transformants were amplified using oWX1555 and oWX1556, and sequenced using odr19 and oML77.

xerD loxP-cat-loxP (BWX3890).

The *loxP-cat-loxP* cassette was inserted downstream of *xerD* by transforming an isothermal assembly reaction containing the following 3 PCR products into PY79: 1) *xerD* and its upstream region (amplified from PY79 genomic DNA using oWX1454 and oWX1617); 2) *loxP-cat-loxP* fragment amplified from pWX465 using universal primers oWX438 and oWX439; 3) the region downstream of *xerD* (amplified from PY79 genomic DNA using primers oWX1486 and oWX1457). The transformants were amplified using oWX1500 and oWX1501, and sequenced using oWX1500 and oML77.

xerD (Y277F) loxP-cat-loxP (BWX3896).

The Y277F point mutation was generated by transforming an isothermal assembly reaction containing the following 2 PCR products into PY79: 1) part of *xerD* and its upstream region (amplified from PY79 genomic DNA using oWX1454 and oWX1618); 2) part of *xerD*, *loxP-cat-loxP*, and the downstream of *xerD* amplified from the genomic DNA of BWX3890 using primers oWX1619 and oWX1457). The transformants were amplified using oWX1500 and oWX1501, and sequenced using oWX1500 and oML77.

xerD (Y277F)-mgfp mut3 spec (BWX3898).

The Y277F point mutation was generated by transforming an isothermal assembly reaction containing the following 2 PCR products into PY79: 1) part of *xerD* and its upstream region (amplified from PY79 genomic DNA using oWX1454 and oWX1618); 2) part of *xerD-mgfp mut3 loxP-spec-loxP*, and the downstream of *xerD* amplified from the genomic DNA of BWX3655 using primers oWX1619 and oWX1457). The transformants were amplified using oWX1500 and oWX1501, and sequenced using oWX1500 and oML77.

xerD-prC spec (BWX3970).

An isothermal assembly reaction containing the following 2 PCR products was directly transformed to PY79: 1) a region containing *xerD* and upstream region (amplified from PY79 genomic DNA using oWX1454 and oWX1642); 2) a region containing *spec* and the downstream of *xerD* (amplified from BWX3655 genomic DNA using primers oWX1643 and oWX1457). This results in the addition of a 5 amino acid linker (LEGSG) and a PrC tag (EDQVDPPRLIDGK) to the C terminus of XerD before the stop codon. The transformants were amplified using oWX1500 and oWX1501 and sequenced using oWX1500 and oML79.

xerC-prC spec (BWX3974).

An isothermal assembly reaction containing the following 2 PCR products was directly transformed to PY79: 1) a region containing *xerC* and upstream region (amplified from PY79 genomic DNA using oWX1448 and oWX1644); 2) a region containing *spec* and the downstream of *xerC* (amplified from BWX3653 genomic DNA using primers oWX1643 and oWX1451). This results in the addition of a 5 amino acid linker (LEGSG) and a PrC tag (EDQVDPPRLIDGK) to the C terminus of XerC before the stop codon. The transformants were amplified using oWX1452 and oWX1453 and sequenced using oWX1452 and oML79.

+26° (XDS)12 loxP-kan-loxP (BWX4004).

The (XDS)12 *loxP-kan-loxP* fragment was inserted at +26° in BWX3370 (Wang et al., 2017) that contains a single *parS* site at -1° using an isothermal assembly reaction that contained 3 PCR products: 1) the region upstream of +26° (amplified from PY79 genomic DNA using oWX1336 and oWX1654); 2) (XDS)12 *loxP-kan-loxP* fragment amplified from the genomic DNA of BWX3970 using universal primers oWX438 and oWX1563; 3) the region downstream of +26° (amplified from PY79 genomic DNA using primers oWX1338 and oWX1339). The transformants were amplified using oWX1340 and oWX1341, and sequenced using oWX1340 and oML83. In some cases, the *loxP-kan-loxP* cassette was removed using a *cre* expressing plasmid pDR244 (Meeske et al., 2015).

-19° (XDS)12 loxP-spec-loxP (BWX4006).

The (XDS)12 *loxP-spec-loxP* fragment was inserted at -19° using an isothermal assembly reaction that contained 3 PCR products: 1) the region upstream of -19° (amplified from PY79 genomic DNA using oWX1648 and oWX1649); 2) (XDS)12 *loxP-spec-loxP* fragment amplified from genomic DNA of BWX3855 using universal primers oWX438 and oWX1563; 3) the region downstream of -19° (amplified from PY79 genomic DNA using primers oWX1650 and oWX1651). The transformants were amplified using oWX1652 and oWX1653, and sequenced using oWX1652 and oML79. In some cases, the *loxP-spec-loxP* cassette was removed using a *cre* expressing plasmid pWX492 (X.W. and D.Z.R., unpublished data).

-109° (XDS)1 loxP-spec-loxP (BWX4201).

An isothermal assembly reaction containing the following 2 PCR products was directly transformed to PY79: 1) a region containing the upstream of 2802 kb region (amplified from BWX3855 genomic DNA using oWX1551 and oWX1729); 2) a region containing *loxP-spec-loxP* and the downstream of 2802 kb region (amplified from BWX3855 genomic DNA using primers oWX439 and oWX1554). This results in retaining a single XDS site from the (XDS)12 array. The transformants were amplified using oWX1555 and oWX1556 and sequenced using oWX1555.

-109° (XDS)2 loxP-spec-loxP (BWX4203).

An isothermal assembly reaction containing the following 2 PCR products was directly transformed to PY79: 1) a region containing the upstream of 2802 kb region (amplified from BWX3855 genomic DNA using oWX1551 and oWX1730); 2) a region containing *loxP-spec-loxP* and the downstream of 2802 kb region (amplified from BWX3855 genomic DNA using primers oWX1731 and oWX1554). This results in retaining two XDS sites from the (XDS)12 array. The transformants were amplified using oWX1555 and oWX1556 and sequenced using oWX1555.

ΔXDS1 (1717kb) loxP-kan-loxP (BWX3709).

An isothermal assembly reaction containing the following 3 PCR products was directly transformed to PY79: 1) the region upstream of *XDS1* (amplified from PY79 genomic DNA using oWX1490 and oWX1491); 2) *loxP-kan-loxP* cassette (amplified from pWX470 using universal primers oWX438 and oWX439); 3) the region downstream of *XDS1* (amplified from PY79 genomic DNA using primers oWX1492 and oWX1493). The transformants were amplified and sequenced using oWX1494 and oWX1495.

ΔXDS2 (1912kb) loxP-spec-loxP (BWX4107).

An isothermal assembly reaction containing the following 3 PCR products was directly transformed to PY79: 1) the region upstream of *XDS2* (amplified from PY79 genomic DNA using oWX1672 and oWX1673); 2) *loxP-spec-loxP* cassette (amplified from pWX466 using universal primers oWX438 and oWX439); 3) the region downstream of *XDS2* (amplified from PY79 genomic DNA using primers oWX1674 and oWX1675). The transformants were amplified and sequenced using oWX1676 and oWX1677.

ΔXDS3 (1989kb) loxP-kan-loxP (BWX4109).

An isothermal assembly reaction containing the following 3 PCR products was directly transformed to PY79: 1) the region upstream of *XDS3* (amplified from PY79 genomic DNA using oWX1678 and oWX1679); 2) *loxP-kan-loxP* cassette (amplified from pWX470 using universal primers oWX438 and oWX439); 3) the region downstream of *XDS3* (amplified from PY79 genomic DNA using primers oWX1680 and oWX1681). The transformants were amplified and sequenced using oWX1682 and oWX1683.

ΔXDS4 (2033kb) loxP-spec-loxP (BWX4139).

An isothermal assembly reaction containing the following 3 PCR products was directly transformed to BWX4125: 1) the region upstream of *XDS4* (amplified from PY79 genomic DNA using oWX1684 and oWX1685); 2) *loxP-spec-loxP* cassette (amplified from pWX466 using universal primers oWX438 and oWX439); 3) the region downstream of *XDS4* (amplified from PY79 genomic DNA using primers oWX1686 and oWX1687). The transformants were amplified and sequenced using oWX1688 and oWX1689. BWX4125 has *XDS2* and *XDS3* deleted.

ΔXDS5 (2597kb) loxP-kan-loxP (BWX4141).

An isothermal assembly reaction containing the following 3 PCR products was directly transformed to BWX4125: 1) the region upstream of *XDS5* (amplified from PY79 genomic DNA using oWX1690 and oWX1691); 2) *loxP-kan-loxP* cassette (amplified from pWX470 using universal primers oWX438 and oWX439); 3) the region downstream of *XDS5* (amplified from PY79 genomic DNA using primers oWX1692 and oWX1693). The transformants were amplified and sequenced using oWX1694 and oWX1695. BWX4125 has *XDS2* and *XDS3* deleted. This strain was generated by successively transforming genomic DNA containing single XDS deletions (described above) and looping out the *loxP-kan-loxP* or *loxP-spec-loxP* using a *cre* expressing plasmids pDR244 (Meeske et al., 2015) or pWX492 (X.W. and D.Z.R., unpublished data).

Strain construction (*E. coli*)

FTR-kan-FRT *P_{XDS1}-lacZ* in *E. coli*.

To construct the *lacZ* reporter repressed by XerD, we used a method described in (Cho and Bernhardt, 2013). Specifically, the chromosomal region of TB10 (Johnson et al., 2004) encompassing the *lacI* gene and *lac* promoter was replaced with a kanamycin resistance cassette (*FTR-kan-FRT*) and a synthetic promoter containing the XerD binding sequence at 1717 kb (*XDS1*) inserted between the -35 and -10 elements of the promoter by λ Red recombinering. An isothermal assembly reaction that contained the following 2 PCR products was transformed to TB10 by electroporation: 1) the region upstream of *lacZ* (amplified from *E. coli* strain HC328 (Cho and Bernhardt, 2013) using oWX1717 and oWX1718); 2) the region containing *lacZ* (amplified from HC328 using oWX1719 and oWX1720). The resulting *E. coli* construct was amplified using oWX1717 and oWX1720 and sequenced using oWX1720. Following recombinering, the *FTR-kan-FRT P_{XDS1}-lacZ* reporter was transduced into MG1655 using P1 phage, resulting cWX1495.

attλ Plac expressing constructs.

pHC886, pWX730, pWX731, pWX732, pWX737 and pWX738 were integrated to *attλ* using methods described in (Haldimann and Wanner, 2001). Specifically, the plasmids were transformed into TB28 (Bernhardt and de Boer, 2004) containing pINT-ts (Haldimann and Wanner, 2001). The integration was confirmed by amplification using oligos *attλ* P1, *attλ* P4, CRIM P2, CRIM P3 (Haldimann and Wanner, 2001). The constructs were transduced into cWX1495 by P1 phage.

Supplemental Information

**XerD unloads bacterial SMC complexes
at the replication terminus**

Xheni Karaboga, Zhongqing Ren, Hugo B. Brandão, Payel Paul, David Z. Rudner, and Xindan Wang

Karaboga_Figure S1

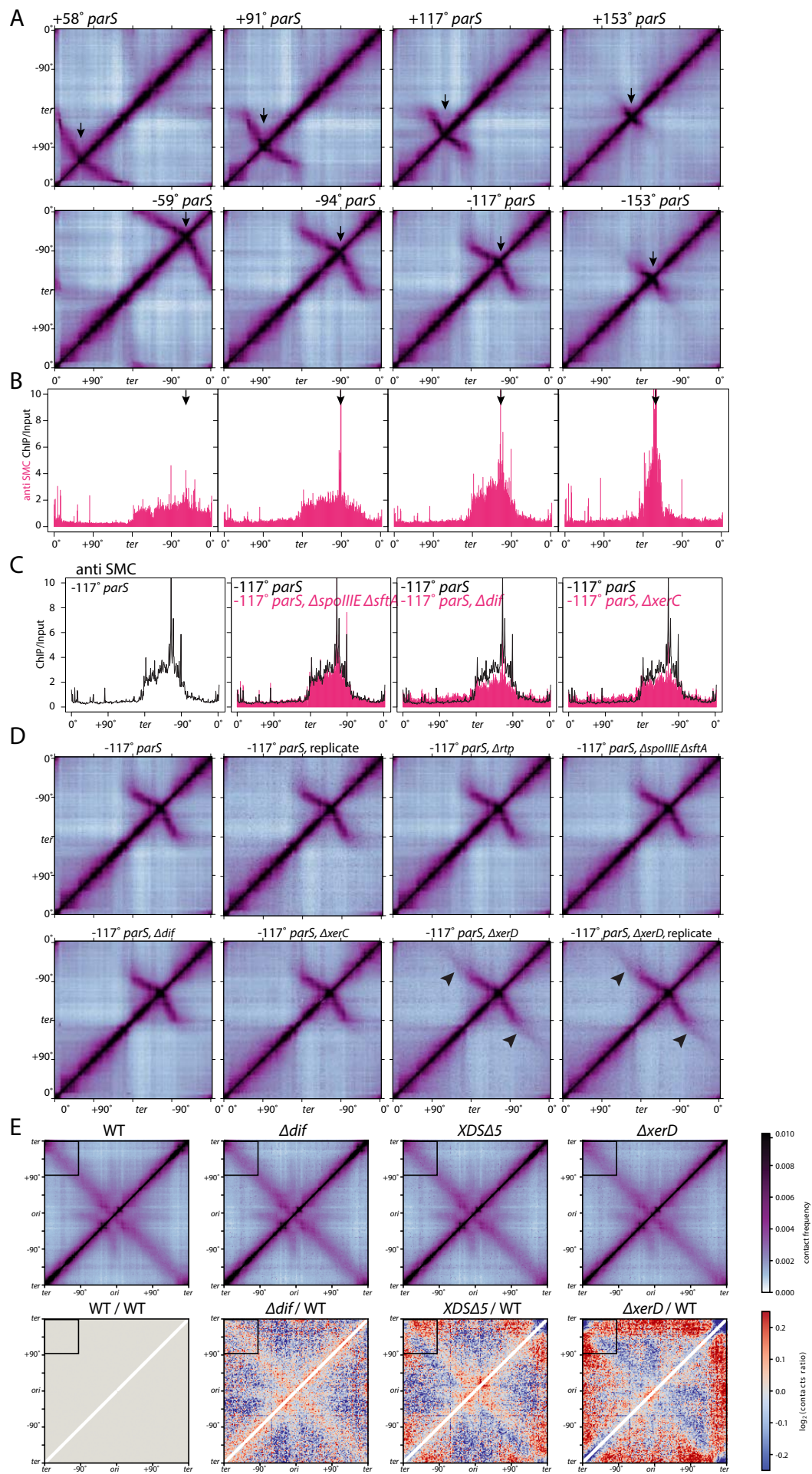
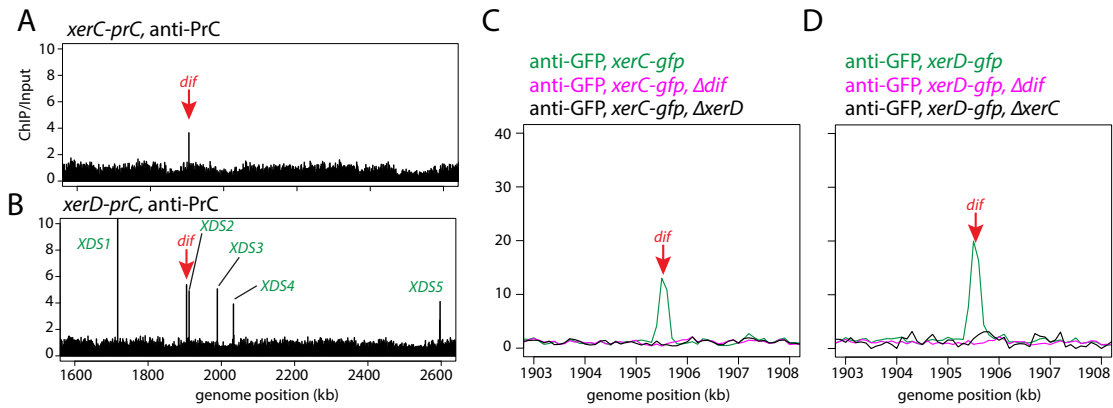


Figure S1. DNA juxtaposition does not extend beyond the terminus region.
Related to Figure 1.

- (A) Normalized Hi-C contact maps of strains harboring single *parS* sites at different genomic locations. Black arrows indicate the positions of *parS* sites.
- (B) Enrichment profiles from anti-SMC ChIP-seq performed in strains containing single *parS* (Wang et al., 2017). Sequencing reads from ChIP and input samples were normalized to the total number of reads. The ChIP enrichment (ChIP/Input) is shown in 10-kb bins. Black arrows indicate the positions of *parS* sites. As we reported previously (Wang et al., 2017), SMC has a cumulative enrichment of 1.24-fold on the terminus-proximal side of an ectopic *parS* site compared to the origin-proximal side. We suspect that head-on encounters between the replisome and/or RNA polymerase and the SMC complexes translocating toward the origin caused the SMC complexes to fall off. In these cases, SMC appears to be non-specifically lost (or unloaded) in an asymmetric manner.
- (C) Enrichment profiles from anti-SMC ChIP-seq performed in strains with the indicated genotypes. Sequencing reads from ChIP and input samples were normalized to the total number of reads. The ChIP enrichment (ChIP/Input) is shown in 10-kb bins. SMC enrichment did not change in $\Delta\text{spollIE}\Delta\text{sftA}$ mutant but showed an intermediate effect in Δdif or ΔxerC , compared to ΔxerD (Fig. 1B). See interpretation in the legend of Fig. S2CD.
- (D) Normalized Hi-C contact maps of the indicated strains. Black carets highlight the DNA juxtaposition that extends beyond the terminus region in ΔxerD in two biological replicates.
- (E) Top, normalized Hi-C contact maps of the wild-type and indicated mutants. Bottom, the ratio of interaction frequencies between the indicated strains plotted in log2 scale. In the wild-type, there is a small gap in the secondary diagonal close to the terminus region indicative of a loss of DNA juxtaposition (black box). This gap is largely absent in strains lacking *XDS* or *XerD*. These data are consistent with the idea that in wild-type, condensin is unloaded by *XerD* bound to *XDS* in the terminus region.

Karaboga_Figure S2

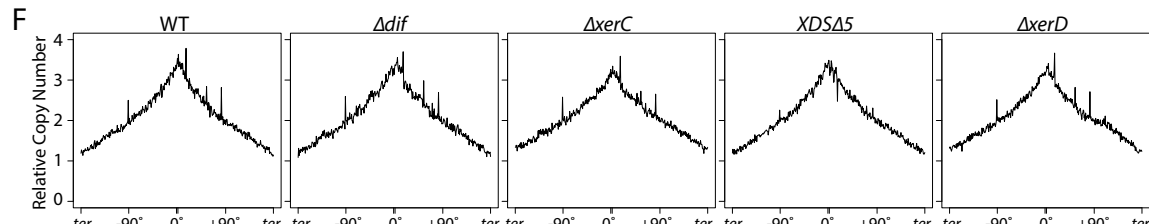


E Statistical test for ChIP-seq peaks

site	Location (bp)	XerD-GFP		XerD-GFP rep2		XerD-PrC		XerC-GFP		XerC-PrC	
		fold	p-value	fold	p-value	fold	p-value	fold	p-value	fold	p-value
<i>dif</i>	1905586	3.30	2.18E-14	2.69	2.22E-16	4.11	2.00E-15	1.99	0.00022	3.04	1.16E-06
<i>XDS1</i>	1717707	8.52	0	5.34	0	10.56	0	1.20	0.18858	1.04	0.45629
<i>XDS2</i>	1912672	3.61	0	3.00	0	4.94	0	1.03	0.24743	1.16	0.26023
<i>XDS3</i>	1989118	3.42	2.03E-13	2.54	2.97E-13	4.59	1.11E-15	0.64	0.79133	0.55	0.75604
<i>XDS4</i>	2033445	5.33	0	3.79	0	4.18	2.02E-13	1.13	0.31109	1.34	0.19395
<i>XDS5</i>	2597186	1.60	0.00492	1.15	0.15614	4.97	0	1.22	0.15509	1.20	0.21706
<i>TerVI</i>	1737897	0.69	0.57194	0.82	0.52675	0.67	0.62734	0.53	0.50015	0.64	0.41677
<i>TerV</i>	1867873	0.77	0.75481	0.91	0.58633	0.63	0.82343	0.92	0.63288	0.58	0.76545
<i>TerVIII</i>	1880336	0.57	0.78212	0.91	0.66046	0.63	0.73523	0.73	0.66881	0.57	0.65635
<i>TerII</i>	1970532	0.67	0.45404	0.88	0.37647	0.93	0.39576	0.72	0.32932	0.71	0.45086
<i>TerI</i>	1970658	0.70	0.45279	0.90	0.37584	1.01	0.39481	0.74	0.32835	0.74	0.44961
<i>TerIII*</i>	1989051	3.38	2.05E-13	2.51	7.65E-13	4.54	1.11E-15	0.64	0.79157	0.55	0.75632

* *TerIII* site is 67 bp away from *XDS5*.

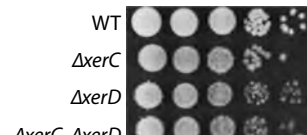
Significant p-values are marked in red.



G

genotype	no. of nucleoids	mean (μ m)	std dev (μ m)	long nucleoids
WT	505	1.34	0.43	0.40%
Δ <i>dif</i>	528	1.45	0.50	2.27%
Δ <i>xerC</i>	560	1.53	0.46	2.32%
Δ <i>XDS5</i>	547	1.65	0.55	4.57%
Δ <i>xerD</i>	507	1.93	0.99	18.93%
Δ <i>XDS5</i> Δ <i>dif</i>	521	2.02	0.94	20.54%
Δ <i>XDS5</i> Δ <i>xerC</i>	508	2.06	0.83	23.23%
Δ <i>XDS5</i> Δ <i>xerD</i>	536	2.36	1.09	33.40%

H



I

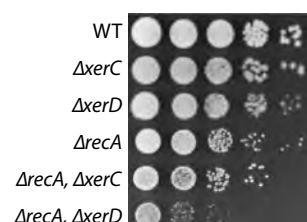


Figure S2. Identification of XerD-specific binding sites. Related to Figure 2 and Figure 3.

(A-B) Enrichment profiles from anti-PrC (Protein C) ChIP-seq performed in strains containing *xerC-prC* (**A**) and *xerD-prC* (**B**). Sequencing reads from ChIP and input samples were normalized to the total number of reads. The ChIP enrichment (ChIP/Input) is shown in 1-kb bins. The positions of the *dif* site and *XDS1-5* sites are indicated.

(C-D) The *dif* region at higher resolution. Normalized ChIP enrichment (ChIP/Input) are plotted in 100-bp bins. **(C)** Anti-GFP ChIP-seq from a *xerC-gfp* strain in otherwise WT (green), or Δ *dif* (magenta), or Δ *xerD* (black). **(D)** Anti-GFP ChIP-seq from a *xerD-gfp* strain in otherwise WT (green), or Δ *dif* (magenta), or Δ *xerC* (black). XerC's enrichment at *dif* requires XerD and *dif*. XerD's enrichment at *dif* requires XerC and *dif*. Our data suggest that XerD directly or indirectly unloads SMC complexes at *XDS* sites and *dif*. Since XerD binding to *dif* requires XerC and *dif*, cells lacking either XerC or *dif* are likely to be partially impaired in unloading and could explain the anti-SMC ChIP-seq profiles observed in these mutants in **Figure S1C**.

(E) Statistical test for ChIP-seq peaks at indicated sites. We performed a statistical test using the Model-based Analysis of ChIP-Seq (MACS) procedure (Zhang et al., 2008). Briefly, the “model” (for the Poisson parameter) is based on the expected number of counts from the neighborhood of a 100-kb window around the site of interest (i.e. *XDS*, *Ter*, or *dif*). The “expectation” parameter of the Poisson is obtained by averaging the ChIP signal of 100 kb around the site of interest. The test value is obtained by the average signal in a small window (1 - 10 kb) around the site. We report the maximum p-value of a list of p-values that were calculated from the Poisson distribution using a 1 kb, 5 kb or 10 kb window. We found that XerD is significantly enriched at *dif* and *XDS1-4* sites in all 3 replicates, and at *XDS5* in 2 replicates. XerD is not significantly enriched at *Ter* sites except for *TerIII* which is 67 bp away from *XDS3*. XerC is significantly enriched at *dif* site in both replicates, and not significantly enriched at *XDS* or *Ter* sites. Significant p-values ($p < 0.05$) are marked in red.

(F) Marker frequency analysis of the indicated mutants. Exponentially growing cells were analyzed by whole genome sequencing. Sequencing reads were normalized by

the total number of reads and plotted in 10-kb bins. We found that replication progression was not altered in these mutants.

(G) Quantitative analysis of nucleoid length measured using MetaMorph (Molecular Devices). “Long nucleoids” are defined as nucleoids greater than 2.64 μ m, which is the (mean + 3x standard deviation) of the wild-type nucleoid length. The distribution of the data is plotted in **Figure 3C**.

(H-I) 10-fold serial dilutions of the indicated strains spotted on LB agar. The $\Delta xerC\Delta xerD$ double mutant grew similarly to $\Delta xerD$ indicating that the growth defect in the $\Delta xerD$ was not due to hyperactive XerC (Cornet et al., 1997). $\Delta recA$ is growth impaired and the $\Delta recA\Delta xerD$ double mutant was even sicker. By contrast, the $\Delta recA\Delta xerC$ double mutant phenocopied $\Delta recA$. Collectively, these data are consistent with idea that XerD has a second function in addition to its role in dimer resolution.

Karaboga_Figure S3

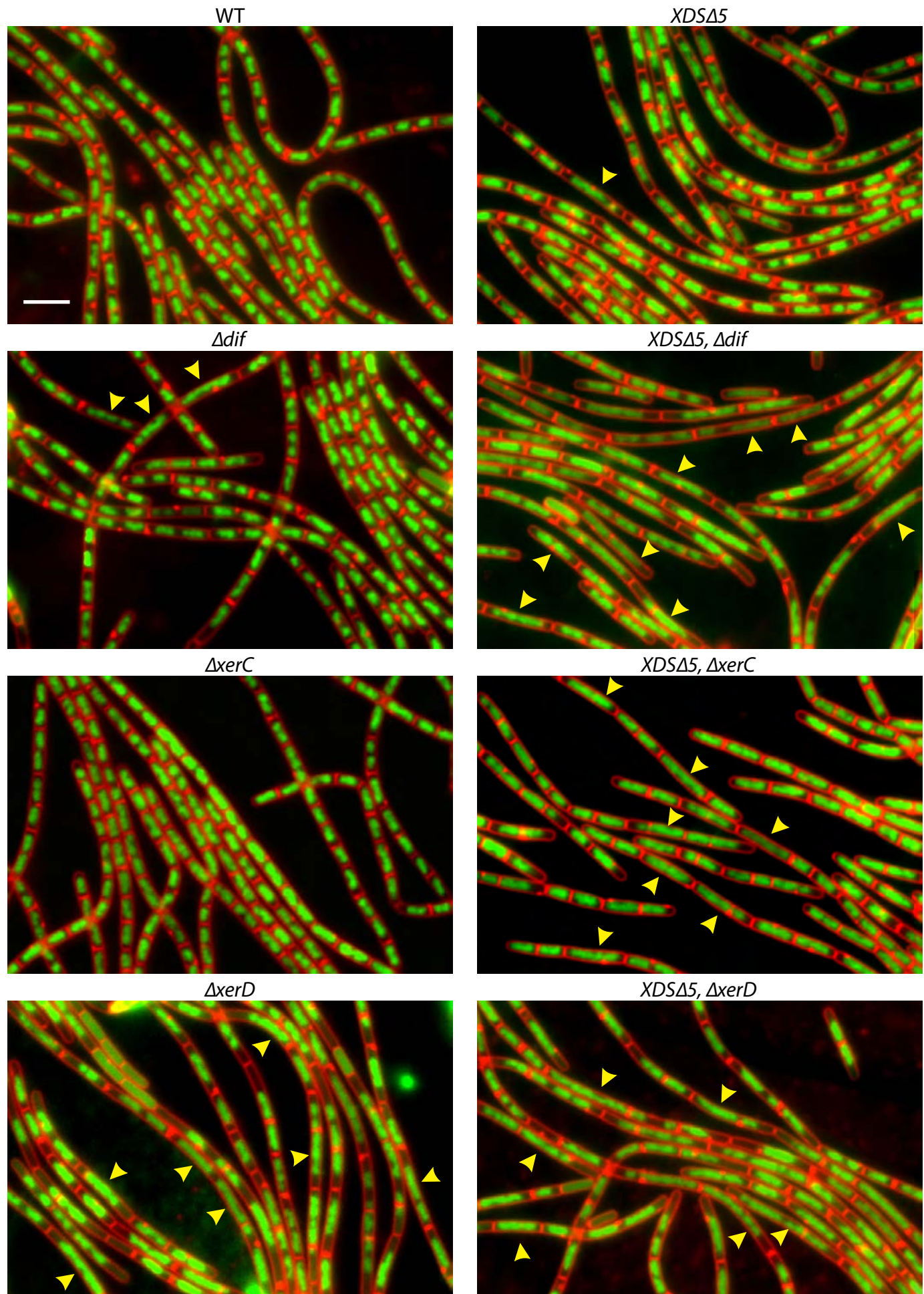


Figure S3. Cytological phenotype of mutants. Related to Figure 3.

Larger fields of the wild-type and mutants in otherwise wild-type strains. DAPI-stained DNA (green) and membranes (red) are shown. Scale bar indicates 4 μ m. Distended nucleoids are highlighted (yellow carets). Quantitative analyses can be found in **Figure 3C** and **S2G**. We note that the nucleoid morphology defect is slightly stronger in cells lacking XerD compared to the *XDSΔ5ΔxerC* or *XDSΔ5Δdif* mutants. We suspect that XerD binds DNA non-specifically in the absence of its binding sites. This weak non-specific binding allows for low-level unloading of the SMC complex and would explain the milder phenotype in strains lacking *dif* and *XDS* sites or *xerC* and *XDS* compared to $\Delta xerD$.

Karaboga_Figure S4

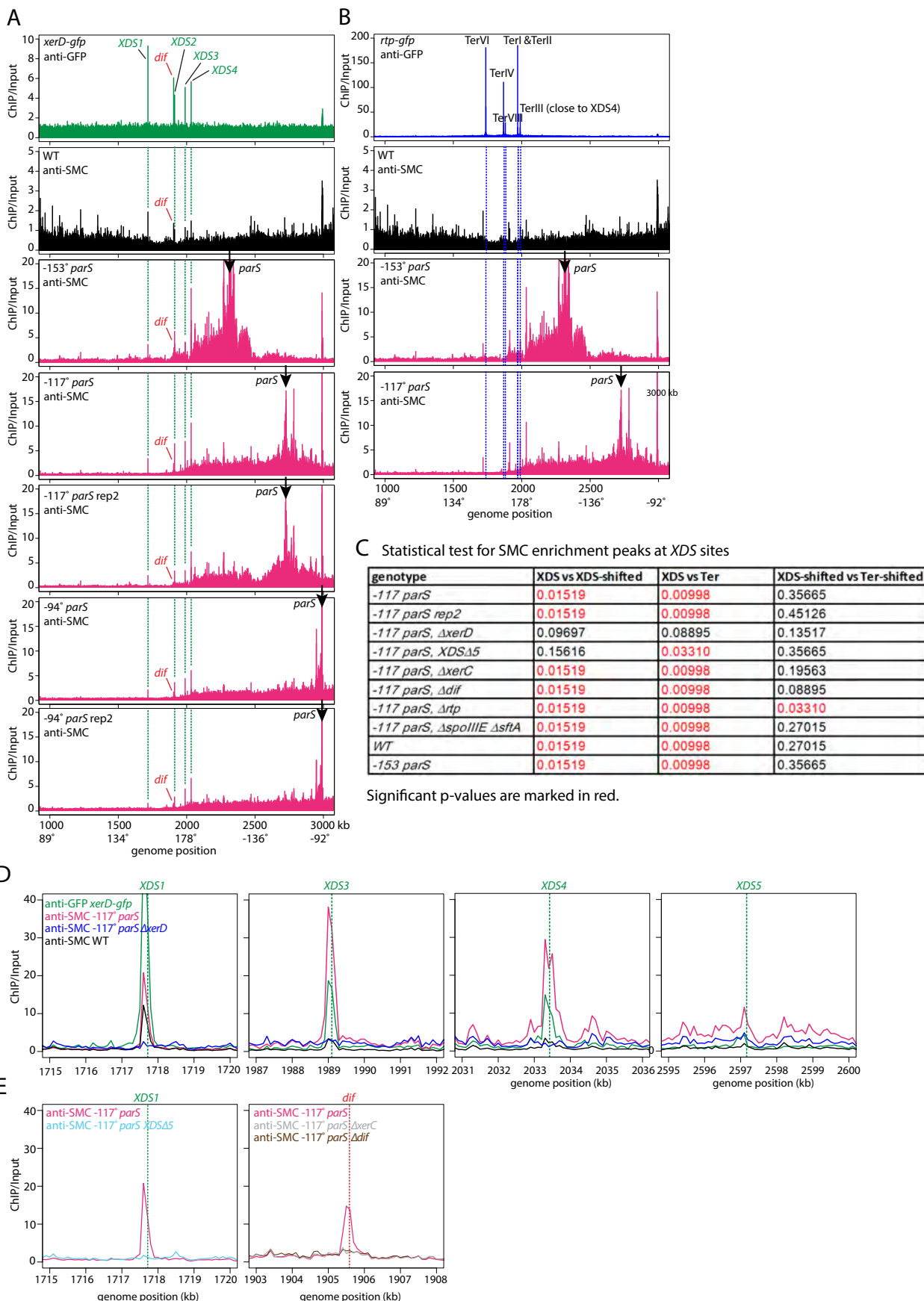
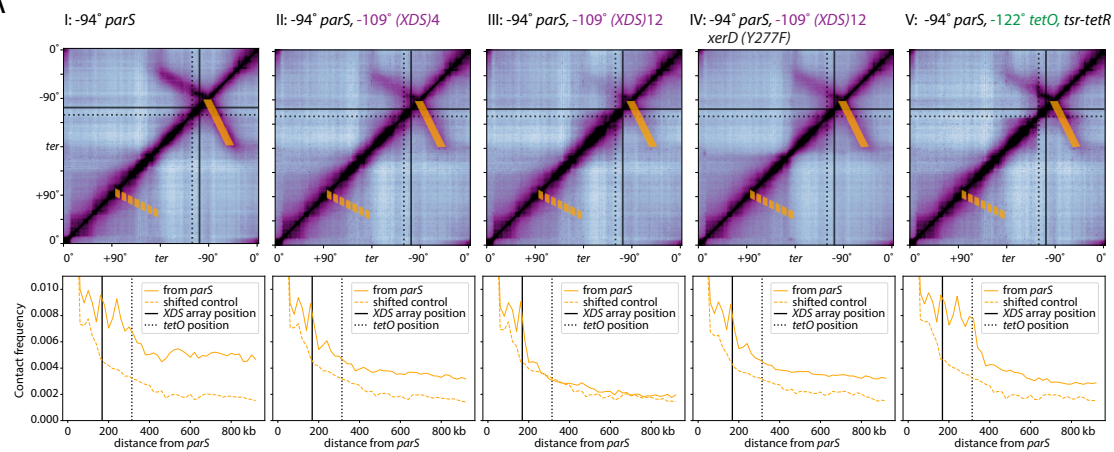


Figure S4. SMC is enriched at XDS sites. Related to Figure 4.

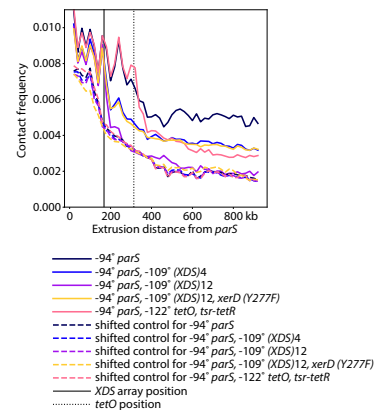
- (A)** Enrichment profile from anti-GFP ChIP-seq (green) performed in a strain containing *xerD-gfp* (top panel). Bottom 6 panels, anti-SMC ChIP-seq performed in wild-type (WT, black), a strain containing a single *parS* site at -153°, a strain containing a single *parS* site at -117° (two biological replicates), or at -94° (two biological replicates). Green dotted lines and black arrows indicate the positions of the *XDS* and single *parS* sites, respectively.
- (B)** SMC is not enriched at *Ter* sites bound by RTP. Top panel, enrichment profile from anti-GFP ChIP-seq (blue) performed in a strain containing *rtp-yfp*. Bottom 3 panels, anti-SMC ChIP-seq performed in WT (black), a strain containing a single *parS* site at -153° or at -117° (magenta). Blue dotted lines indicate the positions of the *Ter* sites.
- (C)** Statistical test for SMC enrichment peaks at *XDS* sites. p-values were computed using a Mann-Whitney U test on ChIP data processed in the following way. 1) We filtered the data by computing a moving average over the ChIP-seq profile with window sizes 1 kb and 100 kb. 2) The 1-kb-filtered profiles were normalized by the 100-kb-filtered profiles. 3) We calculated the normalized signal at the ChIP-seq peak for each *XDS* site, or each *Ter* site. 4) The values obtained from (3) were then used to compute the Mann-Whitney U test to obtain the displayed p-value. The shift size for “shifted controls” was 3000 bp. We found SMC enrichment at *XDS* sites are significantly higher than enrichment at shifted *XDS* sites or *Ter* sites ($p<0.05$), and this significance is dependent on XerD and *XDS*.
- (D)** Enrichment profiles of the genomic regions surrounding *XDS1,3,4,5* at higher resolution. Anti-GFP ChIP-seq performed in *xerD-gfp* (green), anti-SMC ChIP-seq performed in WT (black), or a strain with a -117° *parS* site (magenta) and Δ *xerD* (blue) are shown in the same graph. Normalized ChIP enrichment (ChIP/Input) are plotted in 100-bp bins.
- (E)** Enrichment profile of the genomic region surrounding *XDS1* (left) or *dif* (right). Anti-SMC ChIP-seq performed in a strain containing -117° *parS* with (magenta) or without *XDS* (light blue), *xerC* (gray) or *dif* (brown).

Karaboga_Figure S5

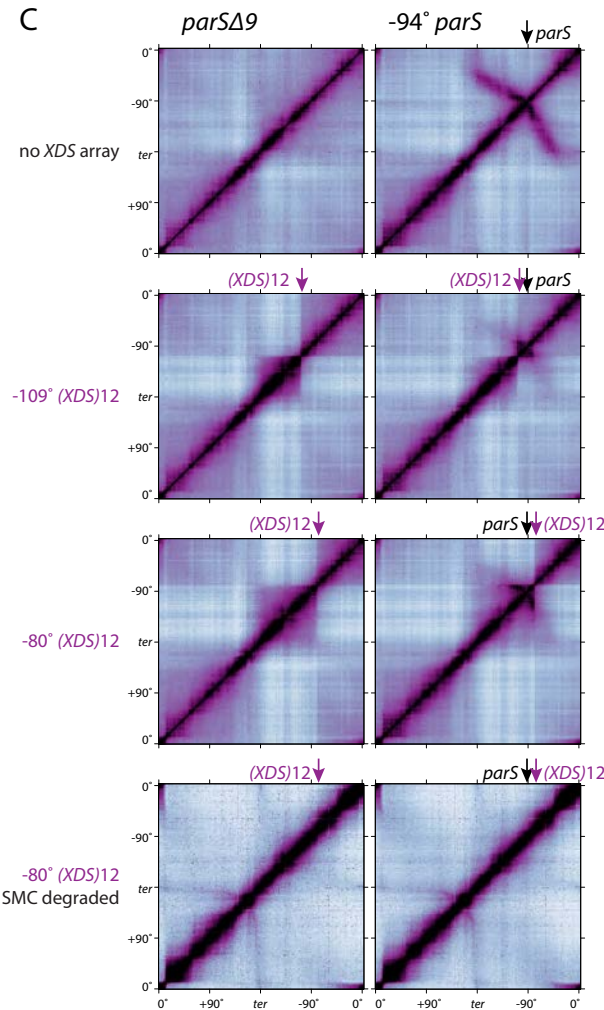
A



B



C



D

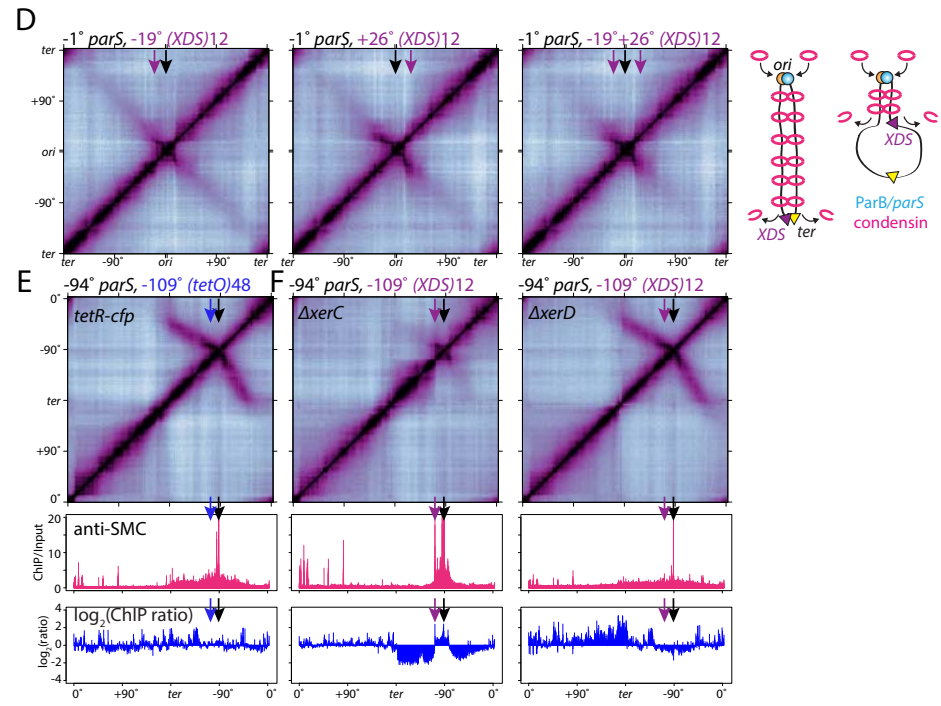


Figure S5. Quantitative analysis of Hi-C results. Related to Figure 5.

(A) Interaction frequencies in the region of chromosome juxtaposition flanking the *parS* site (solid orange parallelogram on the Hi-C map) were plotted for the 5 indicated strains in solid lines on the graph below. For interaction pairs with the same y coordinate in the orange parallelogram, the interaction frequencies were averaged over the 100 kb parallelogram width, and plotted against the distance between *parS* and the y coordinate. As a control, we plotted interaction frequencies of the region in the dashed parallelogram on the Hi-C map in dashed lines on the graph. The control represents the region of interest but mirrored on the opposite chromosome arm; averaging for the control region was done using the x-coordinate because of the mirroring condition.

(B) Data in (A) plotted on the same graph for comparison. For strains II-IV, we found that the interaction frequencies are reduced beyond the position of the *XDS* array. Specifically, strain III (containing WT XerD and (*XDS*)12 array) dropped to the control level, while strain II (containing WT XerD and (*XDS*)4 array) and strain IV (containing XerDY277F and (*XDS*)12 array) dropped to roughly the mid-point (~50%) between the WT and control.

(C) Chromosomal interaction boundaries at (*XDS*)12 arrays require SMC. Normalized Hi-C contact maps of strains lacking all 9 *parS* sites (left) or harboring a single *parS* at -94° (right). The position of the -94° *parS* is indicated (black arrow). Top, both strains lack an ectopic *XDS* array. 2nd panel, both strains contain an *XDS* array (purple arrows) at -109°. 3rd panel, both strains contain an *XDS* array at -80°. Bottom, both strains contain an *XDS* array at -80° and an SMC-degradation system (Griffith and Grossman, 2008; Wang et al., 2014), in which SMC was fused to an SsrA tag, and the *E. coli* adaptor protein SspB that targets SsrA-tagged proteins to the ClpXP proteasome was expressed for 1 hour. Chromosome interaction boundaries are observed at (*XDS*)12 arrays in strains with or without *parS* sites, and these boundaries are absent when SMC is degraded.

(D) Normalized Hi-C contact maps of strains containing -1° *parS*, and an array of 12 *XDS* site inserted at -19° (left), +26° (middle), or both -19° and +26° (right). The positions of *parS* and the *XDS* arrays are indicated by black and purple arrows, respectively. The maps are oriented with the replication origin in the middle of the axes.

Schematic interpretation of data is shown. In wild-type cells, *XDS* sites (purple triangle) that are present at the terminus unload SMC complexes (magenta rings). When an *XDS* array is inserted on one of the chromosome arms, condensin is unloaded from both arms preventing juxtaposition of DNA beyond the array.

(E) Normalized Hi-C contact map of a strain containing a single *parS* at -94°, an array of 48 *tetO* operators at -109°, and expressing *tetR-cfp*. Below the Hi-C map, is an anti-SMC ChIP-seq enrichment profile (magenta), and the ratio of ChIP-seq enrichment relative to -94° *parS* strain plotted in a semi-log graph (blue). The positions of *parS* and the *tetO* array are indicated by black and blue arrows. In contrast to the (*XDS*)12 array, a (*tetO*)48 array did not alter DNA juxtaposition of SMC enrichment.

(F) The loss of DNA juxtaposition and SMC enrichment beyond the *XDS* array requires XerD but not XerC. Hi-C matrices and SMC ChIP-seq enrichment profiles in strains containing -94° *parS*, (*XDS*)12 array at -109°, Δ xerC (left) or Δ xerD (right).

(G) The (*XDS*)12 array does not impair DNA replication. Marker frequency analysis of strains containing a single *parS* at -94° without (left) or with (right) an (*XDS*)12 array at -109°. Sequencing reads for ChIP input samples were plotted. The positions of *parS* and the *XDS* array are indicated by black and purple arrows. The plots are oriented with the replication origin at the center of the x axis.

Karaboga_Figure S6

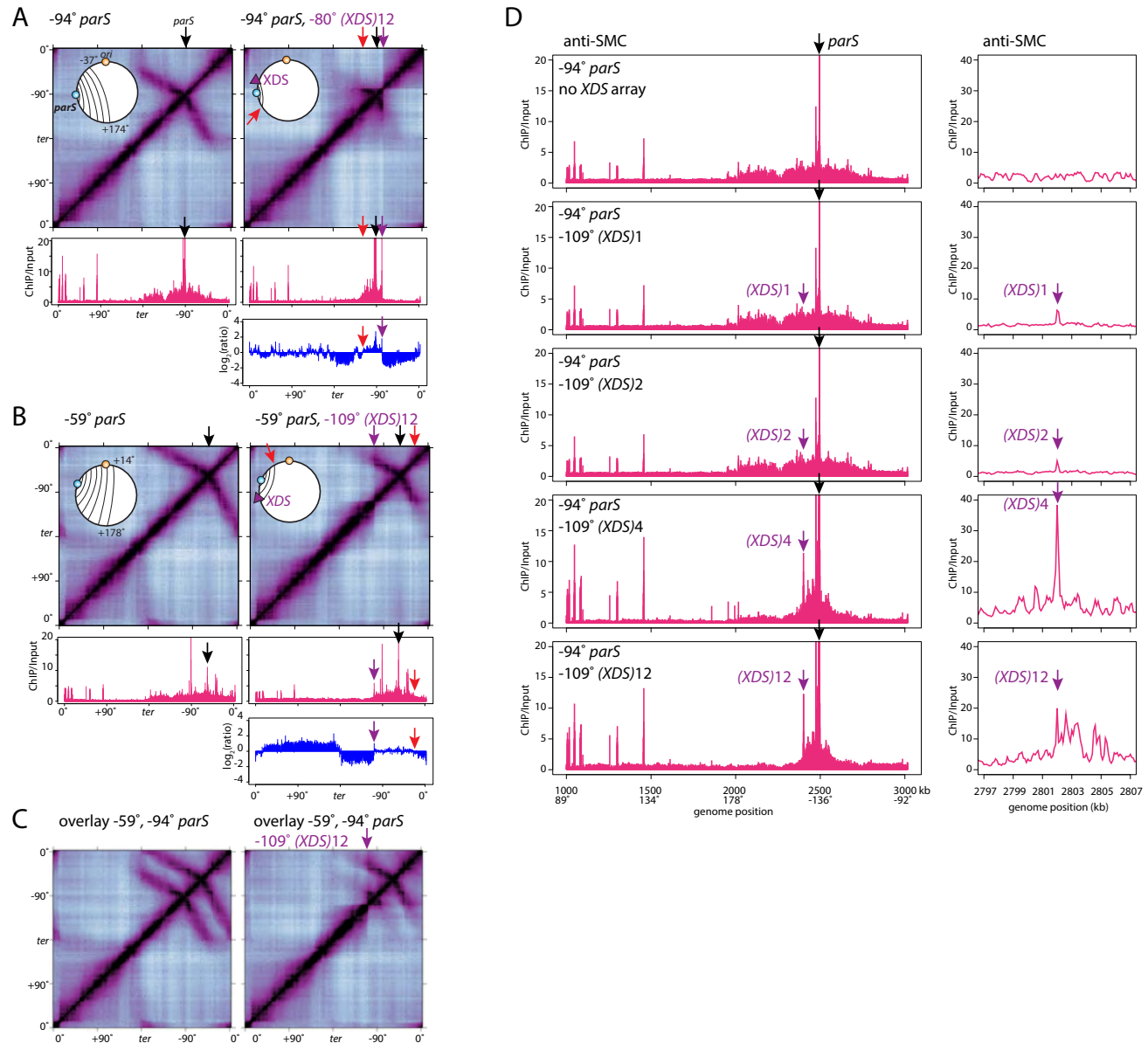


Figure S6. (*XDS*)12 array prevents DNA juxtaposition and SMC enrichment.
Related to Figure 5.

(A-B) Normalized Hi-C contact maps of strains containing a single *parS* at -94° (A, left) and an (*XDS*)12 array inserted at -80° (A, right), or a single *parS* at -59° (B, left) and an (*XDS*)12 array inserted at -109° (B, right). Below each Hi-C map is an anti-SMC ChIP-seq enrichment profile (magenta). The ratio of ChIP-seq between the strains with or without the (*XDS*)12 array is plotted in a semi-log graph (blue). The position of *parS* and the *XDS* array are indicated by black and purple arrows. Red arrows indicate the position that is juxtaposed with the *XDS* array, determined from the Hi-C maps. SMC enrichment is reduced beyond the *XDS* array and the juxtaposed position.

(C) Overlay of two Hi-C contact maps with single *parS* sites at -59° and -94° (left) or with an (*XDS*)12 array at -109° (right).

(D) Comparison of ectopic *XDS* arrays with 1, 2, 4 and 12 sites. Enrichment profiles from anti-SMC ChIP-seq performed in strains containing a *parS* site at -94° and 1, 2, 4, or 12 *XDS* sites at -109°. The left panel shows SMC enrichment profile across the entire genome. The right panel shows a 10-kb region surrounding the -109° locus harboring the *XDS* array. Insertion of one or two *XDS* sites does not significantly reduce SMC enrichment beyond -109°. Consistent with their inability to reduce SMC enrichment beyond -109°, small SMC enrichment peaks were present at these ectopic *XDS* sites. By contrast, insertion of arrays with 4 and 12 *XDS* sites reduced SMC enrichment beyond -109° and its juxtaposed position at -84°. Black and purple arrows indicate the positions of the -94° *parS* site and the -109° *XDS* arrays, respectively.

Karaboga_Figure S7

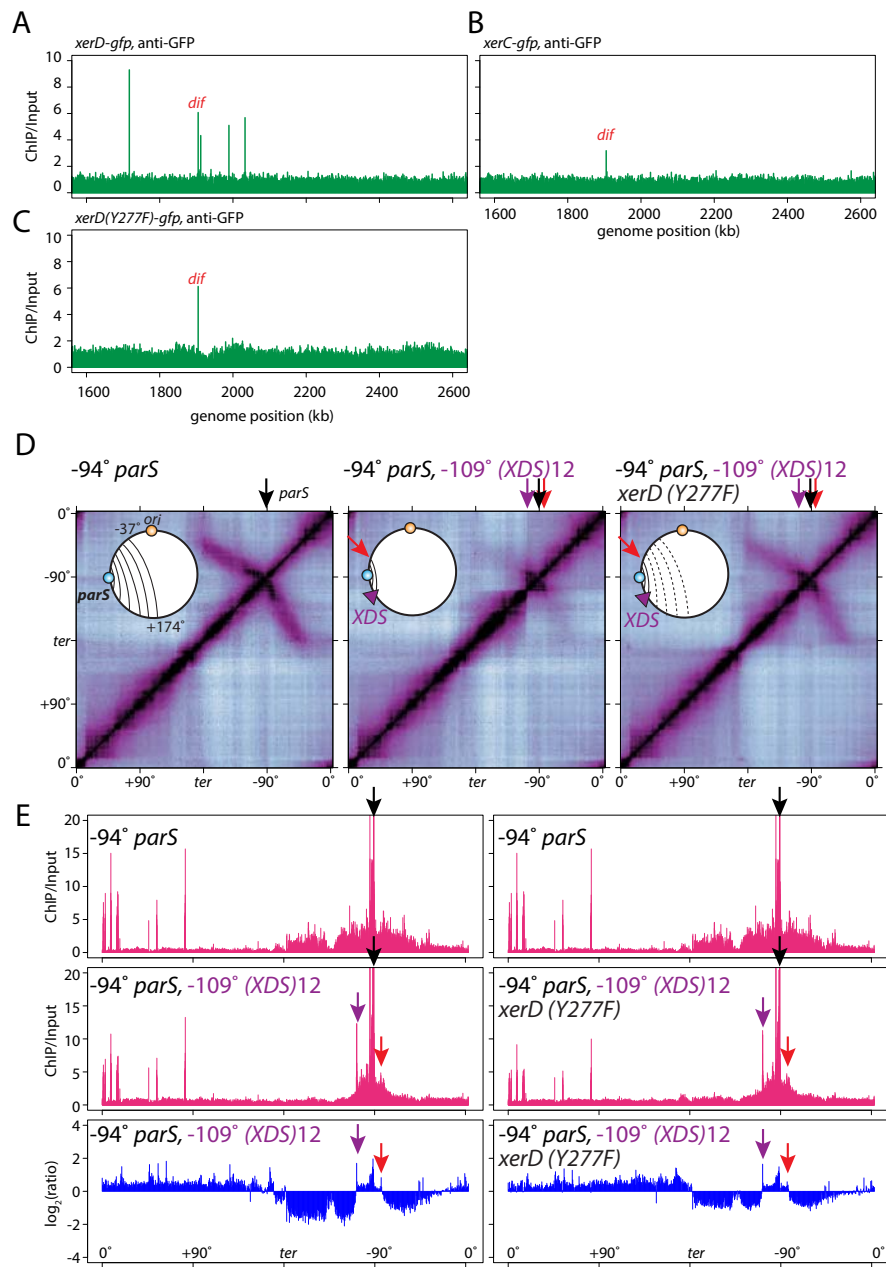


Figure S7. Condensin unloading in XerD catalytic mutant. Related to Figure 7.

(A-C) Enrichment profiles from anti-GFP ChIP-seq performed in cells expressing *xerD-gfp* (A), *xerC-gfp* (B), and *xerD(Y277F)-gfp* (C). XerD(Y277F)-GFP enrichment was only detected at the *dif* site. The loss of enrichment at the *XDS* sites is consistent with the *E. coli* *in vivo* DNA binding assay in **Figure 2E**, in which expression of XerD(Y277F) partially inhibited transcription suggesting its affinity for *XDS1* is lower than wild-type XerD. XerD(Y277F) was enriched at *dif* and we suspect the stronger binding was facilitated by XerC.

(D) Normalized Hi-C contact maps of strains containing -94° *parS* (left), with an (*XDS*)12 array at -109° (middle and right) or with the *xerD(Y277F)* (right). XerD(Y277F) reduced DNA juxtaposition beyond the *XDS* array at -109° and the juxtaposed position at -84°. The partial reduction (~50%, see quantification in **Figure S5AB**) compared to wild-type XerD is consistent with the reduced affinity of XerD(Y277F) for *XDS* sites seen above.

(E) Enrichment profiles from anti-SMC ChIP-seq from the strains in **(D)**. SMC enrichment beyond the (*XDS*)12 array dropped 4 fold in the strain containing wild-type XerD (left, blue) and 2 fold in the strain harboring XerD(Y277F) (right, blue). Thus, comparing to the wild-type, the XerD(Y277F) mutant had a 50% reduction in SMC enrichment outside of the -84° to -109° region, consistent with the ~50% reduction in contact frequency observed in Hi-C (**D**, and **Figure S5AB**). Collectively, these data indicate that the catalytic activity of XerD is not required to unload condensin.